REPUBLIC OF TÜRKİYE

YILDIZ TECHNICAL UNIVERSITY

GRADUATE SCHOOL OF SCIENCE AND ENGINEERING

BIOMIMETIC SYNTHESIS AND CHARACTERIZATION OF CALCIUM PHOSPHATE NANOPARTICLES FOR REGENERATIVE MEDICINE

Musab ORAK

MASTER OF SCIENCE THESIS

Department of Bioengineering

Bioengineering Program

Supervisor

Prof. Dr. Mehmet Murat ÖZMEN

Co-Supervisor

Dr. Sofia DEMBSKI

July, 2024

REPUBLIC OF TÜRKİYE

YILDIZ TECHNICAL UNIVERSITY

GRADUATE SCHOOL OF SCIENCE AND ENGINEERING

BIOMIMETIC SYNTHESIS AND CHARACTERIZATION OF CALCIUM PHOSPHATE NANOPARTICLES FOR REGENERATIVE MEDICINE

A thesis submitted by Musab ORAK in partial fulfillment of the requirements for the degree of MASTER OF SCIENCE is approved by the committee on 31.07.2024 in the Department of Bioengineering, Bioengineering Program.

Prof. Dr. Mehmet Murat ÖZMEN	Dr. Sofia DEMBSKI
Yıldız Technical University	Fraunhofer Institute
Supervisor	Co- supervisor

Approved By the Examining Committee

Prof. Dr. Mehmet Murat ÖZMEN, Supervisor

Yildiz Technical University

Doç. Dr. Emrah Şefik ABAMOR, Member

Yildiz Technical University

Asst. Prof. Cansu NOBERİ, Member

Istanbul Gelisim University

I hereby declare that I have obtained the required legal permissions during data collection and exploitation procedures, that I have made the in-text citations and cited the references properly, that I haven't falsified and/or fabricated research data and results of the study and that I have abided by the principles of the scientific research and ethics during my Thesis Study under the title of "Biomimetic Synthesis and Characterization of Calcium Phosphate Nanoparticles for Regenerative Medicine" supervised by my supervisor, Prof. Dr. Mehmet Murat ÖZMEN. In the case of a discovery of a false statement, I am to acknowledge any legal consequence.

Musab ORAK

Signature

Dedicated to my family and

everyone who contributed with their support

ACKNOWLEDGEMENTS

I would like to give my deepest appreciation and gratitude to my supervisor Prof. Dr. Mehmet Murat ÖZMEN and my co-supervisor Dr. Sofia DEMBSKI who guided me throughout the writing of my master thesis. I would not be able to complete my research without their guidance with valuable knowledge and generous support.

It is my pleasure to express my gratitude to Dr. Tobias WEIGEL and Anika HOEPPEL for their contributions to putting theoretical knowledge into practice and sharing their knowledge about academic writing.

I would like to extend my deepest gratitude to the people of the Department of Bioengineering at Yildiz Technical University for their unwavering support. I would also like to thank the Fraunhofer Institute for Silicate Research ISC and biomaterial group for all the opportunities and friendly working environment they have provided me to carry out my thesis work.

Lastly, I am deeply grateful to my family and friends who have been my support throughout my academic and personal life.

Musab ORAK

TABLE OF CONTENTS

LIST OF SYMBOLS vii
LIST OF ABBREVIATIONS viii
LIST OF FIGURES x
LIST OF TABLES xii
ABSTRACT xiii
ÖZET vx
1 INTRODUCTION 1
1.1 Literature Review 1
1.2 Objective of the Thesis 3
1.3 Hypothesis 3
2 GENERAL INFORMATION 4
2.1 Calcium Phosphate 4
2.2 Bone Remodeling 4
2.3 Bone Tissue Regenerative Methods 6
2.3.1 Natural Bone Grafts 6
2.3.2 Synthetic Bone Grafts 6
2.4 Physiological Mineralization Process and Role of Extracellular Vesicles 8
2.4.1 Extracellular Vesicles 8
2.4.2 Mineralization of the Bone 10
2.5 Isolation Methods of Extracellular Vesicles 11
2.5.1 Ultracentrifugation 11
2.5.2 Polyethylene Glycol Precipitated Ultracentrifugation 12
2.5.3 Density Gradient Centrifugation 13
2.5.4 Size Exclusion Chromatography 13
2.6 3D Printing 15
2.6.1 3D Bioprinting 16
3 MATERIALS AND METHOD 18
3.1 Equipments and Materials 18
3.2 Instructions for Experimental Methodology 22
3.2.1 Calcium Phosphate Nanoparticles Synthesis 22
3.2.2 Extracellular Vesicle Obtaining 24

3.2.3 Calcification Extracellular Vesicles in Collagen Gels 25
3.2.4 Calcification of Collagen-Extracellular Vesicles-Cell Gels 28
3.2.5 3D Bioprinting 29
3.3 Characterization Methods 32
3.3.1 Cell Counting 32
3.3.2 Inductively Coupled Plasma Mass Spectrometry 33
3.3.3 Nanoparticle Tracking Analyzer 33
3.3.4 Staining with Alizarin Red and 4′,6-diamidino-2-phenylindole 33
3.3.5 Transmission Electron Microscopy 34
3.3.6 Scanning Electron Microscopy 34
4 RESULTS AND DISCUSSIONS 35
4.1 Calcium Phosphate Nanoparticles Obtaining 35
4.1.1 Results of Synthesis Process 35
4.1.2 Characterization Results of the Calcium Phosphate Nanoparticles .. 36
4.2 Results of Extracellular Vesicles Isolation 45
4.3 Calcification of Extracellular Vesicles 49
4.4 Calcification of Collagen-Extracellular Vesicles-Cell Gels 51
4.5 3-D Bioprinting Results 60
5 CONCLUSION 62
REFERENCES 64
PUBLICATIONS FROM THE THESIS 71

LIST OF SYMBOLS

kPa	Kilopascal
kV	Kilovolt
µL	Microliter
mg	Milligramm
mL	Milliliter
nm	Nanometer
Mn	Number Average Molecular Weight
g	Relative Centrifugal Force

LIST OF ABBREVIATIONS

AM	Additive Manufacturing
ApoBD	Apoptotic Body
ß-TCP	ß-tricalcium Phosphate
CAD/CAM	Computer-Aided Design/Computer-Aided Manufacturing
CaP	Calcium Phosphate
DAPI	4′,6-diamidino-2-phenylindole
DMEM	Dulbecco's Modified Eagle Medium
DMP1	Dentin Matrix Protein 1
DNA	Deoxyribonucleic Acid
EDTA	Ethylenediaminetetraacetic
EDX	Energy Dispersive X-Ray Analysis
EV	Extracellular Vesicle
FCS	Fetal Calf Serum
GNS	Gel Neutralization Solution
HA	Hydroxyapatite
HCl	Hydrochloric Acid
ICP-MS	Inductively Coupled Plasma Mass Spectrometry
ILV	Intraluminal Vesicle
LaBP	Laser-Assisted Bioprinting
MHDS	Multi-Head Deposition Systems
mRNA	Messenger Ribonucleic Acid
MSCs	Mesenchymal Stem Cell
MV	Microvesicle
MVC	Multivesicular Body
NTA	Nanoparticle Tracking Analyzer
NP	Nanoparticle
PBS	Phosphate Buffered Saline
PCL	Polycaprolactone
PEG	Polyethylene Glycol
PFA	Paraformaldehyde
PLA	Polylactic Acid
PMMA	Polymethyl Methacrylate

SEC	Size Exclusion Chromatography
SEM	Scanning Electron Microscopy
TEM	Transmission Electron Microscopy

LIST OF FIGURES

Figure 2.1 Physiological bone remodeling process 5
Figure 2.2 Options for bone tissue regenerations 7
Figure 2.3 EVs types 9
Figure 2.4 Schematic representation of CaP production from preosteoblast cells in vitro conditions 11
Figure 2.5 Schematic representation of an isolation method using ultracentrifugation 12
Figure 2.6 Schematic representation of the effect of PEG on EV isolation 13
Figure 2.7 Schematic representation of EV isolation with density gradient centrifugation 13
Figure 2.8 Schematic representation of the isolation of substances by SEC 14
Figure 2.9 An example of 3D bioprinting organ 17
Figure 3.1 Schematic representation of the CaP production process 24
Figure 3.2 Schematic representation of EV isolation methods 25
Figure 3.3 Schematic representation of the methodology of the preparation of 5 different types of collagen gels 27
Figure 3.4 Schematic representation of 4 different ways of obtaining gels and CaP production from these gels 28
Figure 3.5 Schematic representation of the steps involved in the 3D bioprinting 31
Figure 3.6 An image taken from the 3D bioprinting process 32
Figure 3.7 3D bioprinted samples 32
Figure 4.1 Light microscopy images of preosteoblast cells 36
Figure 4.2 Concentration (particles/mL) results of CaP NPs obtained with NTA 39
Figure 4.3 Mean size (nm) results of CaP NPs obtained with NTA 39
Figure 4.4 Light microscope images of osteoblast cells at 10X magnification after staining with alizarin red 40
Figure 4.5 Light microscope images of osteoblast cells at 10X magnification after staining with DAPI 41
Figure 4.6 TEM images of CaP NPs obtained in 3D environment 42
Figure 4.7 TEM images of the CaP NPs obtained from preosteoblast donor 1 in 2D environment 44
Figure 4.8 NTA results of EVs obtained with and without PEG precipitation 46
Figure 4.9 ICP-MS results showing the Ca and P ions content of EV and concentrated CaP samples 46
Figure 4.10 Images of collagen-EV gels after staining with alizarin red 49

Figure 4.11 Light microscope images of collagen-EVs gel slides at 10X magnification after staining with alizarin red 50

Figure 4.12 P and Ca ion concentration (mol/L) results of calcified gels obtained by ICP-MS 51

Figure 4.13 P and Ca ion concentration (mol/L) results of calcified EV-cell gels obtained by ICP-MS 52

Figure 4.14 P and Ca ion concentration (mol/L) results of calcified EV gels with and without cells obtained by ICP-MS after 2 weeks of incubation... 53

Figure 4.15 SEM images of the collagen-EV-cell gels..... 55

Figure 4.16 EDX analysis of the collagen-EV-cell gels 57

Figure 4.17 Light microscope images of collagen gels at 20X magnification after staining with alizarin red and DAPI..... 59

Figure 4.18 Light microscope images of bioprinted material samples at 20X magnification after staining with alizarin red and DAPI 61

LIST OF TABLES

Table 2.1 EV isolation techniques 14
Table 3.1 Equipment for synthesis and characterization methods 18
Table 3.2 Chemicals for the syntheses and characterization methods 19
Table 3.3 Chemicals for cell cultures 21
Table 3.4 Cells with donor details 21
Table 3.5 Composition of media and solutions for cell cultures 22
Table 3.6 Components of 3D bioprinting model 30
Table 4.1 Ca/P ratio of samples obtained from 3D environment 37
Table 4.2 Ca/P ratio of donor 1 samples obtained from 2D environment 37
Table 4.3 Size distribution of CaP NPs obtained in 3D environment 43
Table 4.4 Size distribution of CaP NPs obtained in 2D environment from osteoblast cells 44
Table 4.5 EV isolation studies in the literature 48

ABSTRACT

Biomimetic Synthesis and Characterization of Calcium Phosphate Nanoparticles for Regenerative Medicine

Musab ORAK

Department of Bioengineering

Master of Science Thesis

Supervisor: Prof. Dr. Mehmet Murat ÖZMEN

Co- supervisor: Dr. Sofia DEMBSKI

It is a common situation that, as a result of aging and some serious accidents, bone tissue is damaged to an extent that it cannot repair itself. Calcium phosphate (CaP) is commonly used in implants to help heal damaged bone tissue because it makes up the majority of bone. The ease of production and functionalization paves the way for the synthetic production of CaP. During the physiological bone healing process, the CaP particles accumulate in collagen fibrils and crystallize according to the shape of the bone tissue. However, since CaPs in synthetic implants have already grown to a sufficient size and crystallized before interacting with the collagens of the target bone tissue, they cannot accumulate according to the collagen structure of the target tissue and mimic its shape. This leads to compatibility problems between synthetic CaP implants and target bone tissue.

To overcome this problem, in this thesis, physiological CaP production was followed and extracellular vesicles (EVs), which interact with collagens in bone tissue and provide CaP production, were obtained from osteoblast cells. The resulting EVs were then combined with synthetic collagen fibers to form gels, and

the CaP nanoparticle (NP) production potential of the gels was investigated by incubation. Finally, in a novel aspect of this thesis, an artificial bone matrix was innovatively prepared using collagen, EVs, and human osteoblast cells. Subsequently, bone-like samples were produced from this bone matrix using a 3D bioprinter. Since the aim of this study was to investigate the ability of EVs to produce CaP in a biomimetic manner in bone-like samples, the bioprinted samples were incubated for 4 weeks and tested for CaP production.

The synthesized EVs and CaP NPs were characterized by ICP-MS, NTA, SEM, TEM, and alizarin red and DAPI staining, and their structural morphology and contents were investigated. Isolated EVs were found to have an average size of 227 ± 32 nm in the NTA results. According to the ICP-MS results, no Ca and P ions were found in the EVs samples, indicating that the EVs were isolated before being converted to CaP. After 2 weeks of incubation, the formed gels were characterized by SEM, alizarin red staining and ICP-MS, and the interaction of EVs with collagens was observed. As a result of this interaction, the biomimetic CaP production of the gels was observed. Accordingly, CaP nanoparticles were obtained, generally in spherical form, with sizes varying between 49 nm and 490 nm. The alizarin red and DAPI results showed that human osteoblast cells maintained their viability in the 3D bioprinted samples, while also confirming that EVs successfully synthesized CaP biomimetically. By using the EVs obtained in biomimetic bone regeneration studies, it is anticipated that they have the potential to overcome biocompatibility issues, and thus effectively mimic the target bone.

Key Words: Biomimetic, calcium phosphate, extracellular vesicle, nanoparticles, bioprinting, collagen

ÖZET

Rejeneratif Tıpta Kalsiyum Fosfat Nanopartiküllerinin Biyomimetik Sentezi ve Karakterizasyonu

Musab ORAK

Biyomühendislik Anabilim Dalı

Yüksek Lisans Tezi

Danışman: Prof. Dr. Mehmet Murat ÖZMEN

Eş-Danışman: Dr. Sofia DEMBSKI

Yaşlanma ve bazı ciddi kazalar sonucunda kemik dokusunun kendini onaramayacak kadar zarar görmesi sık görülen bir durumdur. Kalsiyum fosfat (CaP) kemiğin büyük bir kısmını oluşturduğundan, hasarlı kemik dokusunun iyileşmesine yardımcı olmak için implantlarda kullanımı oldukça yaygındır. Üretim ve işlevselleştirme kolaylığı, CaP'ın sentetik üretiminin önünü açmaktadır. Fizyolojik kemik iyileşmesi sürecinde, CaP mineralleri kolajen fibrillerde birikerek kemik dokusunun şekline göre kristalleşir. Ancak sentetik implantlardaki CaP'ların, hedef kemik dokusunun kolajenleri ile etkileşime girmeden önce zaten yeterli boyuta ulaşıp kristalleşmiş olmaları, hedef dokunun kolajen yapısına göre birikip şeklini taklit edememeleri ile sonuçlanmaktadır. Bu da sentetik CaP implantları ile hedef kemik dokusu arasında uyumluluk sorunlarına yol açmaktadır.

Bu sorunun üstesinden gelebilmek amacıyla, bu tezde fizyolojik CaP üretimi takip edildi ve kemik dokusundaki kolajenlerle etkileşime girerek CaP üretimini sağlayan hücre dışı keseciklerin (EV'ler) insan osteoblast hücrelerinden izolasyonu sağlandı.

Elde edilen EV'ler daha sonra sentetik kolajen fiberler ile birleştirilerek jeller oluşturuldu ve inkübasyon yoluyla jellerin CaP nanopartikül (NP) üretim potansiyelleri araştırıldı. Son olarak, bu tezin özgün bir yönü olarak, kolajen, EV'ler ve insan osteoblast hücreleri kullanılarak yenilikçi bir şekilde yapay bir kemik matrisi hazırlandı. Sonrasında bu kemik matrisinden 3 boyutlu biyoyazıcı yardımıyla kemik benzeri numuneler üretildi. Bu çalışmanın amacı EV'lerin kemik benzeri numunelerde biyomimetik bir şekilde CaP üretme yeteneğini araştırmak olduğundan, biyoyazıcı ile oluşturulmuş numuneler 4 hafta boyunca inkübe edildi ve CaP üretimi açısından test edildi.

Sentezlenen EV´ler ve CaP NP'leri; ICP-MS, TEM, NTA, SEM, alizarin kırmızısı ve DAPI boyama ile karakterize edilerek yapı morfolojisi ve içerikleri araştırıldı. NTA sonuçları, izole edilen EV'lerin ortalama 227 ± 32 nm boyutunda olduğunu gösterdi. ICP-MS sonuçlarına göre EV örneklerinde Ca ve P iyonlarına rastlanmadı, bu da EV'lerin CaP'a dönüştürülmeden önce izole edildiğinin göstergesidir. Oluşturulan jeller, 2 haftalık inkübasyondan sonra SEM, alizarin kırmızısına boyama ve ICP-MS ile karakterize edilerek EV´lerin kolajenler ile etkileşimi gözlemlendi ve bu etkileşim sonucunda jellerin CaP ürettiği gözlendi. Buna göre boyutları 49 nm ve 490 nm arasında değişen genellikle küresel formda CaP nanopartikülleri elde edildi. Alizarin kırmızısı ve DAPI sonuçları, insan osteoblast hücrelerinin 3D biyobaskılı kemik benzeri örnekler içerisinde canlılığını koruduğunu gösterirken aynı zamanda EV´lerin başarılı bir şekilde biyomimetik olarak CaP sentezlediğini de ortaya koydu. Elde edilen EVlerin, biyomimetik kemik rejenerasyon çalışmalarında kullanılarak biyouyumluluk sorunlarının üstesinden gelme potansiyeline sahip olduğu ve etkili bir şekilde hedef kemik doku yapısını taklit edebilecekleri düşünülmektedir.

Anahtar Kelimeler: Biyomimetik, kalsiyum fosfat, hücre dışı vezikül, nanopartiküller, biyobaskı, kolajen

1 INTRODUCTION

1.1 Literature Review

Bone tissue can become damaged and dysfunctional due to accidents or aging. Bone tissue has the ability to repair and regenerate itself, but this ability is reduced with age. In some cases where the injury exceeds a critical size, it may be necessary to use a bone tissue implant model to help regeneration and remodeling [1].

The first applied solution is the transfer of natural bone structures from other donors to the patient [2]**.** The transfer of natural tissue in this way is called natural bone grafting [3]. The donor can be the patient itself [4] (autograft) or another member of the same species [5] (allograft). In later studies, members of different species (xenografts) were also accepted as donors. Because the bone structure of dogs, pigs and sheep is similar to that of humans, these animals have often been used for xenografting [6].

Although autografts are the best option in terms of biocompatibility, the biggest obstacle is that have a difficult methodology, and can only be produced in limited quantities [4]. Recently, allografts have shown great development as an alternative to autografts due to the greater number of potential donors while maintaining high biocompatibility. These properties have made allografts the most popular candidate for bone reconstruction in Europe. So much so that it has reached levels comparable to those in America, where approximately 800.000 allografts are used each year [7]. Although they are biocompatible, the risks of disease transmission are too great to ignore. This paves the way for allografts to continue to be viewed with suspicion [5]. In addition to animals commonly used for xenotransplantation, such as sheep and pigs, corals also have been evaluated for bone grafting in studies dating back to 1970 [8]. However, due to poor clinical outcomes in the past and the high risk of disease transmission, xenotransplantation has been almost completely abandoned [9].

The limited number of natural bone grafts and the long and complicated procedures have led to the search for various alternatives for bone grafts such as synthetic bone models. Synthetic materials, isolated cells, tissue scaffolds and growth factors can

be used for synthetic bone models [1]. The number of synthetic bone grafts used for the treatment of serious bone injuries is expressed in millions per year [10]. A calcium phosphate (CaP) ceramic study conducted by Monroe and colleagues in 1971 [11] is considered one of the pioneering studies in this field. Since then, CaP ceramics have been increasingly developed in bone repair studies and their properties have been improved [12]. Recent studies [13] have shown that synthetic CaP implant models also help to promote the formation of new tissues when it is bound to damaged bone. In studies conducted by Hongjian Zhou and colleagues [14] on rabbits, new bone tissue formation was observed after synthetic CaP implantation.

During the physiological bone healing process, extracellular vesicles (EVs) that are released from osteoblast cells trigger CaP production when they interact with the collagen fibers of the bone tissue. The produced CaP particles accumulate in collagen fibrils and crystallize according to the shape of the target bone tissue [13]. The fact that synthetic CaP implant models can be produced cheaply and quickly, is one of the main reasons why they have been studied for so many years [15]. However, because CaPs in synthetic implants have already reached a sufficient size and crystallized before interacting with the collagens of the target tissue, they cannot accumulate according to the collagen structure of the target tissue and mimic its shape. This leads to compatibility problems between synthetic CaP implants and target bone tissue [16]. Because they induce CaP production, the use of EVs in bone regeneration studies has the potential to overcome this compability problem. EVs are secreted by many cells in the body for various purposes other than bone regeneration [17]. Although there are many studies in the literature to isolate EVs from various cell types using many methods such as ultracentrifugation, polyethylene glycol (PEG) precipitation, and size exclusion chromatography [18], studies on their isolation from osteoblasts or mesenchymal stem cells (MSCs) for bone regeneration are quite limited. In the study by Börger and colleagues [19], the PEG precipitation technique was used to isolate EVs from MSCs, which are the undifferentiated version of osteoblast cells. In addition, in the study by Al-Sharabi and colleagues [20], EVs were isolated from MSCs and successful bone regeneration studies were performed in rats using these EVs. As a unique aspect of this thesis, Evs that isolated from human osteoblast cells by PEG

precipitation and non-PEG precipitation methods were combined with synthetic collagen fibers and osteoblast cells to create an artificial bone matrix. This artificial bone matrix was then used to fabricate bone-like specimens using a 3D bioprinter, and the biomimetic CaP synthesis of the bioprinted specimens was investigated.

1.2 Objective of the Thesis

The aim of this study is to develop a new approach to mimic the physiological production of CaP by extracting EVs from osteoblast cells prior to their conversion into CaP.

To achieve this;

- Growth and proliferation of pre-osteoblast cells by incubation with growth medium,
- Isolation of EVs from osteoblast cells by standard ultracentrifugation and PEG-precipitated ultracentrifugation methods,
- Combining EVs with collagen fibers to form gels and incubating the gels with differentiation medium to produce CaP NPs,
- Fabrication of 3D bone-like bioprinted samples using a synthetic collagen matrix consisting of isolated EVs, synthetic collagen fibers and osteoblast cells, and incubation of the bioprinted samples with differentiation medium to produce CaP NPs,

were targeted.

1.3 Hypothesis

We hypothesize that in bone regeneration studies, when the isolated EVs interact with the target tissue, biomimetic CaP synthesis would be possible by achieving mineral growth that matches the structure of the target tissue.

2
GENERAL INFORMATION

2.1 Calcium Phosphate

The majority (60%) of human bone is composed of CaP minerals. They provide physical strength and mechanical stiffness to the bone. The average adult human body contains approximately 1-2 kg of CaP. 99% of this is stored in bones and teeth, with the remainder in muscle, blood and other tissues. As well as being found in bone structure, Ca is also found in the circulatory system and tissues, while P is an important component of DNA and protein. These minerals play an important role in the health of bones, muscles, blood and nerves. CaP minerals also act as a reservoir, providing Ca and P to the extracellular fluid when sufficient Ca cannot be obtained from the kidneys and small intestine [21]. The presence of CaP in bone was first documented in 1769 by Albee and their colleagues [22]. Although CaP is most commonly used in dental and bone implants, it is also widely used in tissue engineering and drug delivery systems. It is also used as an additive in the food industry and as a source of P in agriculture. CaP exists in several forms depending on the Ca/P molar ratio. The most common and used forms are hydroxyapatite (HA) and ß-tricalcium phosphate (ß-TCP) [23, 24].

HA is the most common form of CaP found in biological structures, with the chemical formula $Ca_{10}(PO_4)_6(OH)_2$. CaP minerals found in the structure of bones and teeth are mostly in the form of HA. HA can also be produced synthetically and is often used in synthetic bone grafts due to its biocompatibility, robust mechanical strength, high osteoconductivity and porosity. It is also used as a filling material in the dental field and as a surface coating material for metal implants in order to increase their biocompatibility and integration capability [25].

ß-TCP is a synthetically produced form of CaP which has a higher biodegradation than HA. Its chemical formula is $Ca_3(PO_4)_2$. In addition to synthetic bone and hip grafts, it is used as a scaffold in other biomedical applications [26].

2.2 Bone Remodeling

Bone modeling consists of 2 processes: bone formation and bone resorption. Although they are opposite processes, they can occur simultaneously on different

surfaces of the same bone. This means that these 2 processes can occur without any connection [27].

Bone also acts as a Ca and P reservoir. It is necessary to continuously remodel the bone to prevent bone tissue accumulation and to provide CaP hemostasis. In this way, the mechanical strength of the bone is adjusted to external factors and stimuli. In the process of bone remodeling, damaged or old bone is broken down and removed by osteoclast cells and replaced by new bone that is formed by osteoblast cells [28].

Bone remodeling occurs mainly in adults and involves 5 main steps as shown in Figure 2.1[29]:

1. Activation: Pre-osteoclast cells differentiate into mature osteoclast cells through the interaction of cytokines and growth factors.

2. Resorption: Matrix of old bone is degraded by osteoclast cells.

3. Reflection: Preosteoblast cells are activated after old bone debris is removed from the bone surface.

4. Formation: New bone matrix is formed by osteoblast cells.

5. Quiescence: At this stage, the new bone is lined by osteoblast cells.

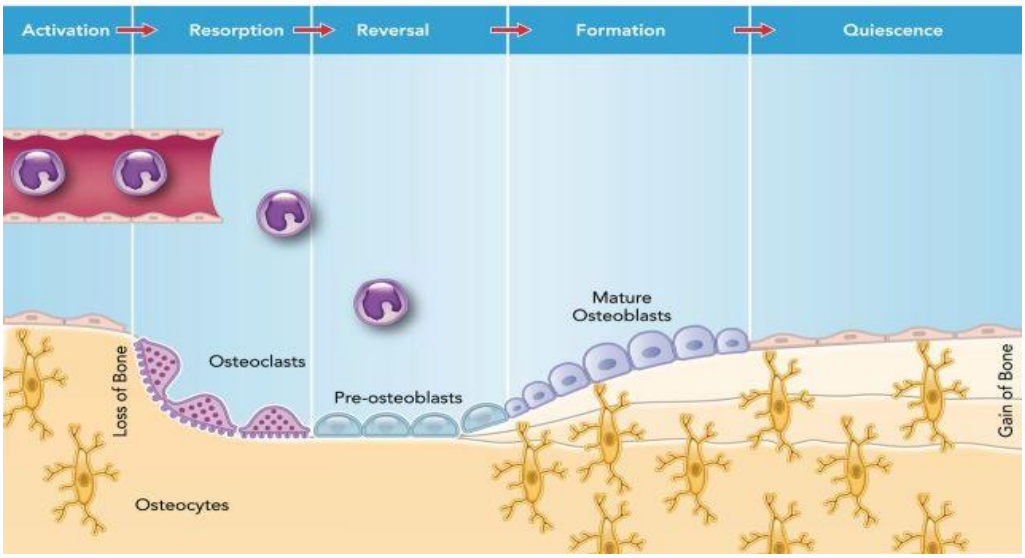


Figure 2.1 Physiological bone remodeling process. Schematic representation of activation, resorption, reflection, formation, and quiescence steps [29].

2.3 Bone Tissue Regenerative Methods

Bone grafting is a medical procedure that relies on the transplantation of a new bone model to rebuild or repair damaged bone. It is important for the bone graft to adapt to the tissue it is transplanting in order to contribute to the physiological healing process. In addition, one of the expected roles of bone grafts is to address the aesthetic problems associated with bone damage. Therefore, it is necessary to understand bone biomechanics for effective treatment [15, 30]**.**

2.3.1 Natural Bone Grafts

Grafts taken from one living organism and transplanted into another are defined as natural grafts. The donor organism can be either of the same species or of a different species. Although high biocompatibility and the ability to mimic the physiological calcification process stand out as the biggest advantages of natural bone grafts, the limited number of donors and the long and costly process are the prominent disadvantages [15].

2.3.2 Synthetic Bone Grafts

Donor limitations for autografts and allografts, and the risk of immune rejection due to pathogens that may originate from the original tissue for xenografts, stand out as the greatest limitations of natural bone grafts. Synthetic bone grafts are produced to overcome these problems. They are designed to mimic the mechanical and biological properties of bone as closely as possible. CaP ceramics are often used as the main material in the structure of these grafts. Polymers such as polymethyl methacrylate (PMMA) and metals such as titanium and nickel are used to improve mechanical properties. In addition, growth factors and bone-forming cells such as osteoblasts and mesenchymal stem cells can be incorporated into the structure of the graft to support the physiological healing process [15]. Different techniques of bone regeneration methods are illustrated in Figure 2.2.

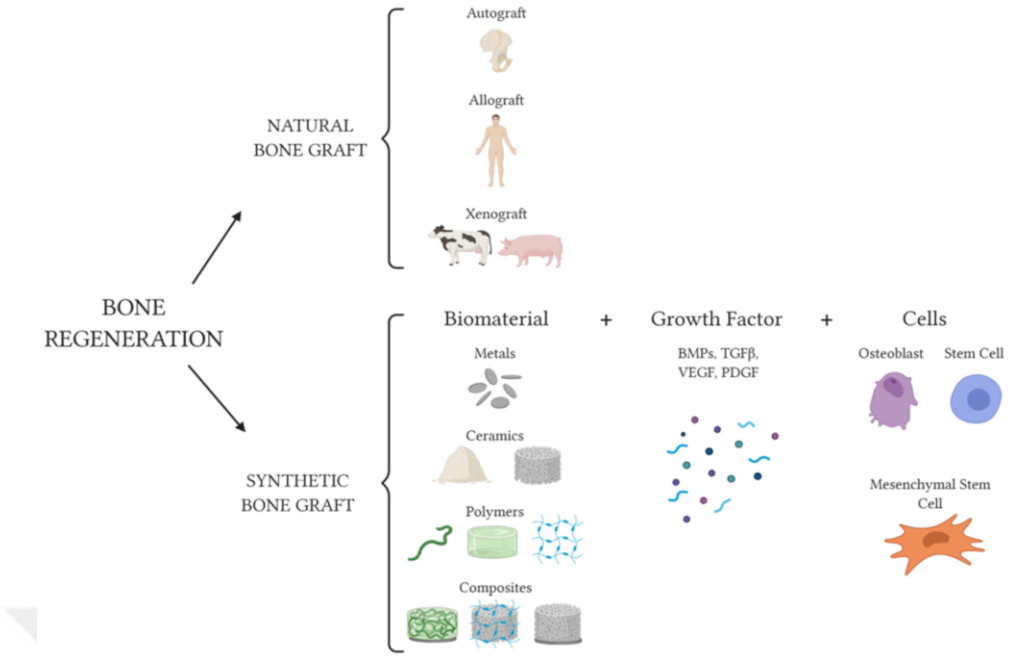


Figure 2.2 Options for bone tissue regenerations. Autografting, allografting and xenografting can be used as alternatives for natural bone graft. Biomaterials can be used to create synthetic bone grafts by functionalizing them with biological agents such as cells and growth factors [31].

Synthetic CaP materials have been used and commercialized in clinical research such as bone grafting, coatings and other implant studies since the early 20th century [25]. They are attracting attention in this field because they are non-toxic and have a high degree of biocompatibility. HA and ß-TCP forms are the most commonly produced types [26, 25]. A study by V.P. Orlovskii and colleagues [32] found that synthetic HA ceramics can effectively bind to the target bone tissue and have no negative impact on the process**.** The biological behavior of HA-based bone grafts is determined by factors such as pore size and microstructure [32]. Despite all the advantages of synthetic bone grafts, which are easy, fast, and inexpensive to produce, mechanical failures and biocompatibility problems arise from their inability to mimic the mineral structure of the tissue in which they are implanted. In a clinical study conducted by W. Linhart and colleagues [33], it was observed that patients who underwent synthetic CaP implantation developed long-term biocompatibility problems**.**

2.4 Physiological Mineralization Process and Role of Extracellular Vesicles

2.4.1 Extracellular Vesicles

EVs are membrane-enclosed structures secreted by various cells. It was originally thought that EVs were only used to remove waste products from cells**.** However, recent studies show that they also enable communication between cells and play a role in physiological processes by transporting substances**.** Proteins, lipids, mRNA and DNA are some of the metabolites transported in this way [17]. EVs also have the potential to take up and process substances from the environment. For example, EVs released from osteoblast cells play an effective role in bone formation by capturing Ca and P ions from the environment [16]. Therefore, EV isolation from osteoblast cells is used in bone regeneration. Since they are released by many cells, their production is considered as an alternative for biological studies [34]. They can be produced by cells in two different ways: First, they can be formed by the substance to be transported arriving at the cell membrane and being trapped in a piece of the membrane and released directly. Second, they can be formed inside the cell membrane and released from the cell membrane when they reach a sufficient size. As shown in Figure 2.3, EVs can be classified into 3 different groups, i.e., exosomes, microvesicles, apoptotic bodies based on their size and the way they are released**.**

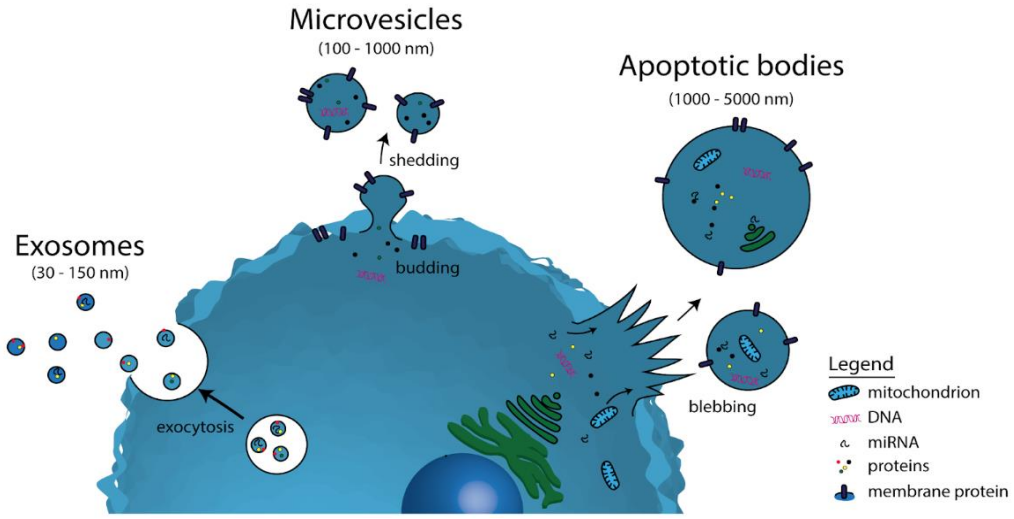


Figure 2.3 EVs types. Microvesicles (100-1000 nm) and apoptotic bodies (1000-5000 nm) are formed directly from the cell membrane during secretion, while exosomes (30-150 nm) are formed inside the cell and then released [35].

2.4.1.1 Exosomes

Exosomes are a subset of EVs ranging in size from 30 to 120 nm. They are secreted indirectly from the cell membrane and are specific to the cells that produce them. The main role of exosomes is to enable communication between cells and tissues by carrying molecules [36]. Their small size allows them to reach deep tissues.

Exosomes are formed by the differentiation of the early endosome, which is formed by budding inward from the plasma membrane. Early endosomes bud inward to form numerous intraluminal vesicles (ILVs). These ILV-containing early endosomes are called multivesicular bodies (MVCs) or late endosomes. MVCs transform into different end products depending on their content and destination. After the early endosome becomes an MVC, the MVC can travel to the lysosome and be eliminated via the trans-Golgi network, or it can travel to the plasma membrane and be secreted from the cell by exocytosis. These secreted MVCs are known as exosomes [37].

2.4.1.2 Microvesicles

Microvesicles (MVs) are formed by budding from the cell membrane. Their size ranges from 100 to 1000 nm. They are used by a wide variety of cells to transport different cargoes such as lipids, microRNAs, proteins and mRNAs. MVs contact

and deliver cargo to recipient cells through specific receptor-ligand interactions [38].

2.4.1.3 Apoptotic Bodies

Apoptotic bodies (ApoBDs) and other EVs differ in origin, lipid structure, release mode, protein markers and, most importantly, the role they play. Unlike exosomes and microvesicles, ApoBDs are secreted by dying cells in the final phase of apoptosis. It is proposed that ApoBDs are produced by these cells to increase the efficiency of waste removal. In this way, they are thought to play a critical role in minimizing the impact of cells undergoing apoptosis on surrounding tissues. ApoBDs have diameters between 50 and 5000 nm, making them the largest EV [39].

2.4.2 Mineralization of the Bone

Bone formation is thought to be related to EVs secreted by osteoblast cells. EVs facilitate this process by providing an environment in which Ca and P concentrations can increase. Once secreted from osteoblast cells, EVs bind to collagen fibers. They take up Ca and P ions from the environment and form CaP mineral precursors in the form of HA. These precursors are released from the EVs into the collagen spaces by rupture of the EV membrane when sufficient concentrations are reached. They then enter the collagen spaces. HA mineral deposition begins in the interstices between the ends of the collagen fibrils [16, 40]. There is no definitive information on how EVs promote HA mineralization in specific regions of collagen, as they do not appear to target collagen fibril ends directly.

HA crystals enlarge and their impurity level decreases as the bone matures. Both growth and aggregation cause crystal enlargement. The initial nucleation of the crystals may be facilitated by the macromolecules of the bone. These macromolecules increase the concentration of Ca and P ions by separating them. They also bind to the surface of the growing crystals to determine the shape, size, and number of crystals. Mineralization promoters, also known as nucleators, include bone sialoprotein and dentin matrix protein 1 (DMP1). Type 1 collagen is not a nucleator, although it is a critical structure of the bone matrix. Mineralization is regulated by alkaline phosphatase and phosphoprotein kinases. Alkaline

phosphatase can increase P concentration by removing HA crystal growth inhibitors or by switching phosphoproteins to control their nucleating ability [40].

Taking into account the physiological mineralization process, it is possible to produce CaP from preosteoblast cells in vitro as illustrated in Figure 2.4. In the first step, preosteoblast cells are cultured in a growth medium for about 2 weeks and transformed into osteoblast cells. In the second step, EVs can be obtained from osteoblast cells within 2-3 days using differentiation medium. If the EVs obtained at this stage are kept in the differentiation medium, they start to produce CaP by collecting free Ca and P ions from the medium [20].

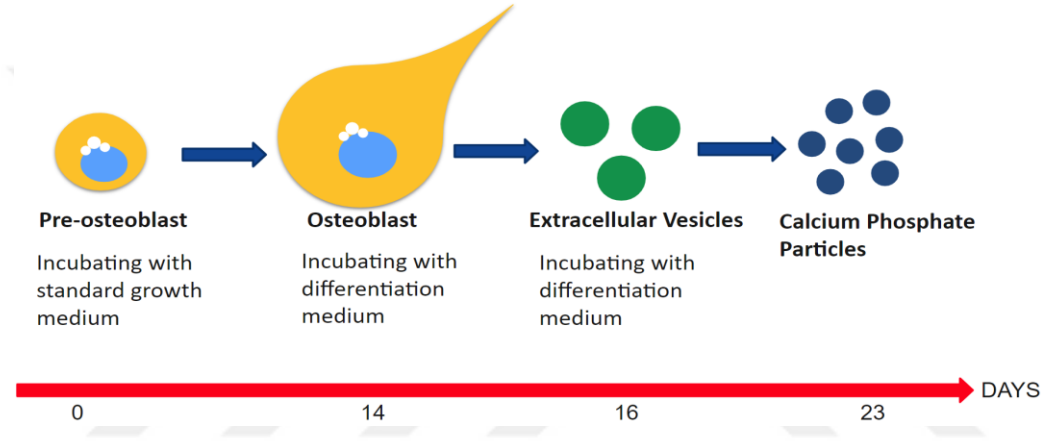


Figure 2.4 Schematic representation of CaP production from preosteoblast cells in vitro conditions

2.5 Isolation methods of Extracellular Vesicles

After obtaining EVs in liquid solution, it is critical to isolate them before using them in studies. Isolation methods can be used to achieve both a high concentration of EVs and to increase the purity of the EVs by eliminating other particles in the liquid. This maximizes the efficiency of the work to be done with EVs [18].

Isolation methods can be applied based on the properties of the substance, such as size and charge [18]. The most commonly used methods to isolate EVs are ultracentrifugation, sucrose density gradient centrifugation, polyethylene glycol (PEG) precipitation and size exclusion chromatography (SEC).

2.5.1 Ultracentrifugation

An ultracentrifuge is a device designed to rotate samples placed inside it at very high speeds, allowing the heavier substances in the samples to precipitate and settle to the bottom as shown in Figure 2.5. Isolating the substances by settling them to

the bottom using this device is called ultracentrifugation**.** Although it is a simple method, the difficulty of achieving a high level of efficiency stands out as its most significant drawback [41].

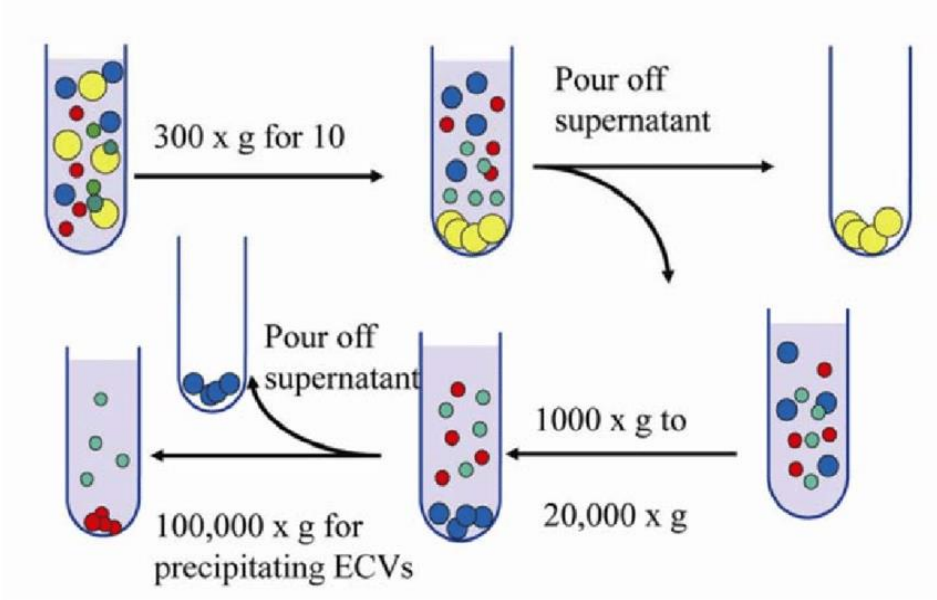


Figure 2.5 Schematic representation of an isolation method using ultracentrifugation. Depending on the rotational force applied, the heavier substances sink to the bottom while the lighter substances remain in the supernatant at the surface. Isolation is achieved by removing the supernatant from the environment. Isolation sensitivity can be improved by increasing the rotational force [42].

2.5.2 PEG Precipitated Ultracentrifugation

The addition of PEG to the isolation liquid is a commonly used method to enhance EV isolation. Since PEG is a highly hydrophilic polymer, it opens up into long chains in water, and the oxygen atoms in the chains bind to H^+ molecules of water. Upon dissolution, the PEG molecules interact with the water molecules around the EVs to form polymer networks [43]. As depicted in Figure 2.6, the resulting polymer networks surround the EVs and limit their contact with water. This reduces the water solubility of the EVs and makes them more susceptible to precipitation. It is simple, inexpensive and efficient, but the increase in efficiency depends on the use of large sample volumes.

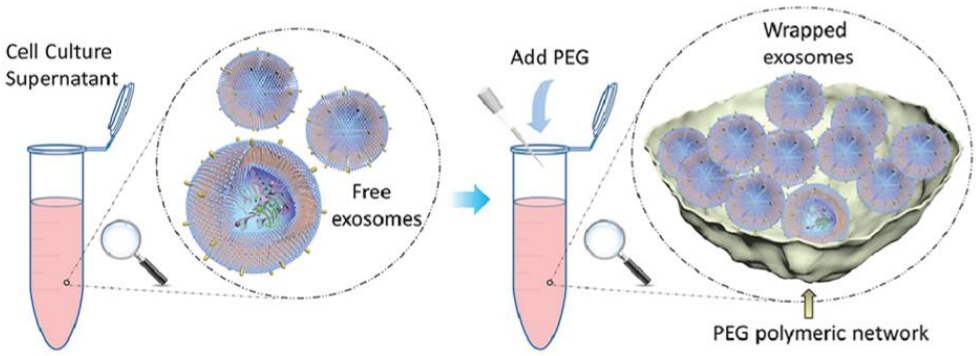


Figure 2.6 Schematic representation of the effect of PEG on EV isolation [43]

2.5.3 Density Gradient Centrifugation

Density gradient centrifugation is a technique used to separate substances according to their density. The isolated EVs are placed in iodixanol solution and are gradually separated according to their density as revealed in Figure 2.7. This method allows EVs to be separated more specifically by size, but the length and complexity of the method is the biggest barrier to its use [44].

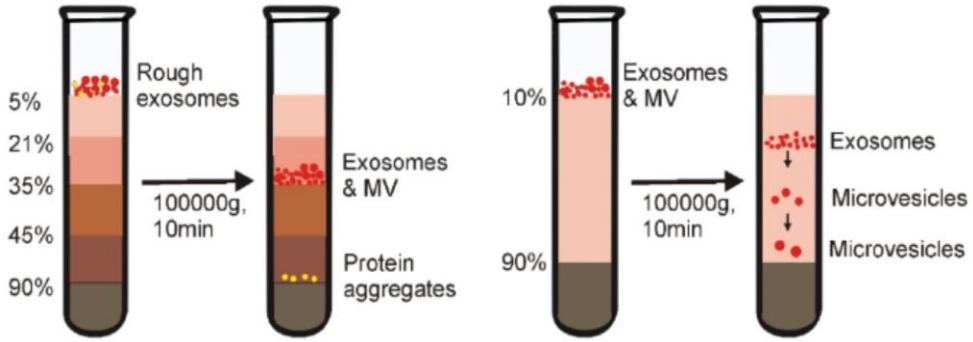


Figure 2.7 Schematic representation of EV isolation with density gradient centrifugation [45]

2.5.4 Size Exclusion Chromatography

SEC is a controlled separation technique used to isolate substances in solution using average pore size characteristics as basically illustrated in Figure 2.8. SEC can also be used to determine the average molecular weight distribution of substances in solution using column calibration**.** With this method, separation can be performed with high precision. In addition, high efficiency can be achieved since the substances do not interact with the stationary phase. However, due to the short scale of the chromatogram, only a limited number of bands can be used, which prolongs the processing time [46].

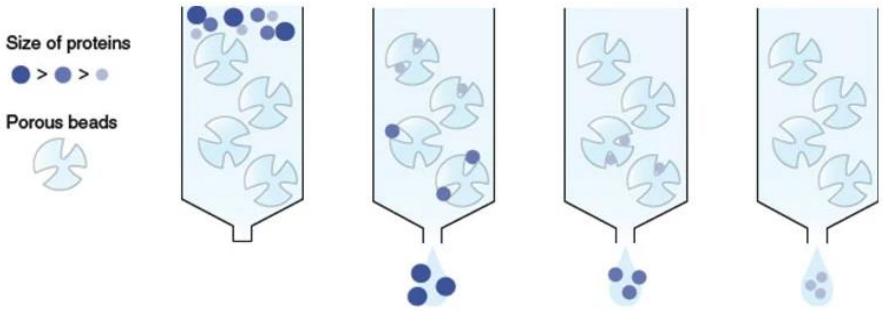


Figure 2.8 Schematic representation of the isolation of substances by SEC. Larger compounds pass more quickly through the porous gel beads and drip off the bottom of the elution column [47].

EV isolation techniques are summarized in Table 2.1 with basic information such as equipment, chemicals, and advantages and disadvantages.

Table 2.1 EV isolation techniques

	Ultra-centrifugation	**Sucrose Density Gradient Centrifugation**	**Size-exclusion Chromatography**	**PEG Precipitation**
Based on	Size-Density	Density	Size	Size-Density
Devices – Materials	Optima L7-65 ultracentrifuge SW40 swing-out rotor	810R centrifuge 10 mL Ultra-Clear centrifuge tubes Optima L7-65 ultracentrifuge SW40 swing out rotor Fluorescence microscopy with Axio Observer.D1 platform (Zeiss SW45 swing-out rotor Microscopic slides Sucrose density gradient	5810R centrifuge 10 mL Ultra-Clear centrifuge tubes Optima L7-65 ultracentrifuge SW40 swing out rotor 16/60 HiLoad Superdex 200 prep grade	500 mL conical centrifuge flasks Avanti J-26XP centrifuge Swing-out rotor JS-5.3 70 mL polycarbonate centrifuge bottles Optima L7-65 ultracentrifuge Tight angle rotor Ti45
Chemicals	PBS	PBS NaCl	PBS NaCl Sodium phosphate	PBS PEG NaCl

Table 2.1 EV isolation techniques (continued)

Advantages	Simple procedure Short procedure (5-6 hours) [18]	Possible to sort much smaller particles for increased specificity High purity can be obtained High yield (70-90%) [18]	Good sensitivity because of having narrow bands and well-defined separation times No sample loss because solutes do not interact with the stationary phase Short procedure (3-4 hours) High yield (70-90%) [18]	Cost-effective High efficiency Moderate yield (60-80%) [18]
Disadvantages	Low yield (50-70%) [18]	More complex than differential centrifugation Long procedure (20-26 hours) [18]	Limited number of bands can be used because of having short scale of chromatogram [18]	Efficiency increased with using higher volume of samples Long procedure (16-18 hours) [18]

2.6 3D Printing

3D printing can be defined as an additive manufacturing (AM) type used to fabricate a variety of geometric shapes. In this process, sequential layers are printed on each other using a model input. 3D printing is widely used in many industries, including dentistry, prototyping, and biomaterial construction. It was quickly embraced by engineers and architects for its cost-effective and time-saving properties, enabling the creation of practical and aesthetic models. There is widespread acceptance that the 3D printing manufacturing system has many advantages over traditional manufacturing. Easier fabrication of complex structures, requiring less materials, allowing personalization in design are the most

prominent advantages of 3D printing. In addition, the ease of using a wide variety of materials, such as concrete, metals, ceramics and polymers, expands the scope of 3D printing [48, 49].

2.6.1 3D Bioprinting

The manufacture of biological products from various building blocks such as biomaterials, cells, tissues, and bioactive molecules is called 3D biofabrication. Electrospinning, particulate leaching, microengineering and lyophilization are the traditional biofabrication methods [50]. Although these techniques can produce 3D structures, their versatility and reproducibility are their main limitations [51].

As an alternative to these existing techniques, 3D bioprinting has recently emerged. Due to its high reproducibility and control over the tissue architectures to be produced, 3D bioprinting has rapidly gained popularity among biofabrication methods [52]. In this method, 3D structures are created by bioink deposition according to previously prepared geometric patterns. As shown in Figure 2.9, many 3D tissue structures, including artificial organs, can be fabricated in this way [53]. 3D bioprinting may involve a variety of techniques, including inkjet bioprinting, extrusion bioprinting, and laser-assisted bioprinting (LaBP) [54].

In addition, computerized bioprinting systems have been developed to increase the specificity of the application. It is important to crosslink the bioinks in a short time so that the patterns, which are produced according to the 3D building models created by computer-aided design/computer-aided manufacturing (CAD/CAM), can stabilize and take their final shape [54].

The selection of bioinks depends on the bioprinter and the application to be used. It is very important that the bioink has suitable properties such as mechanical durability, biocompatibility with natural tissues, and adjustable stabilization and gelation for bioprinting [55, 56].

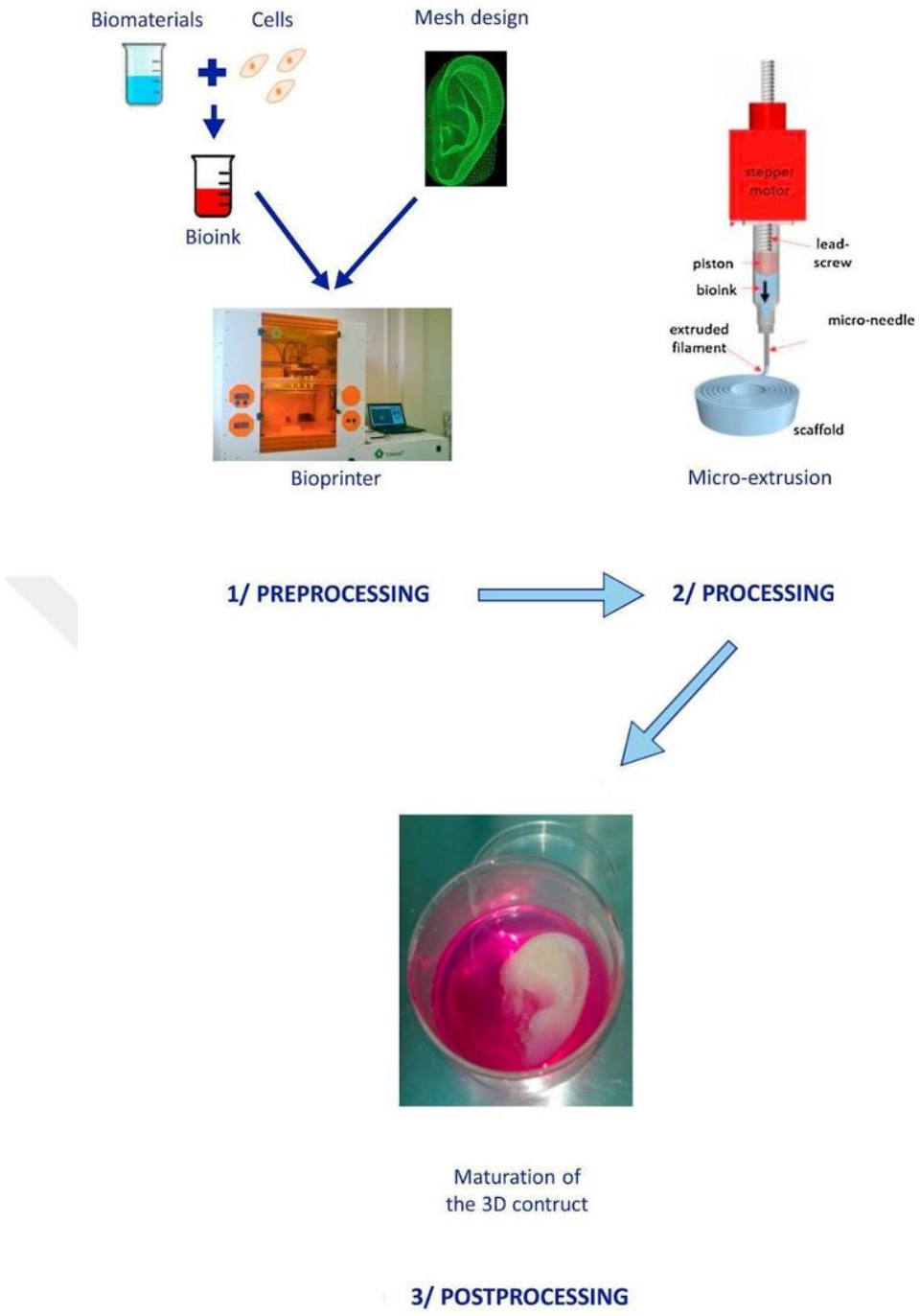


Figure 2.9 An example of 3D bioprinting organ [57]

3
MATERIALS AND METHOD

3.1 Equipments and Materials

Table 3.1 Equipment for synthesis and characterization methods

Device	**Manufacturer**
Water Bath WB14	Memmert
Incubator BBD 6220 CO_2	Thermo Scientific™
Microbiological Safety Cabinet Herasafe KS18	Thermo Scientific™
Centrifuge Megafuge 40R	Heraeus
Centrifuge Z 513 K	Hermle
Ultracentrifuge L80 XP	Beckman Coulter
Bioprinter The R-GEN 200	Regen-Hu
Cell Culture Microscope DMi 1	Leica
ICP-MS, iCAP RQ	Thermo Fisher Scientific
Thermomixer pro	Cell Media
Nanoparticle Tracking Analyzer Basic NTA-PMX-120	ZetaView®
Analytical Electron Microscope JEM2100	JEOL
Vortex 4 Basic	IKA
SEM Micrograph Supra 25	Zeiss
Sliding Microtome SM2010R	Leira

Table 3.1 Equipment for synthesis and characterization methods (continued)

Modular Paraffin Embedding Center TES Valida	MEDITE
Fluorescence Microscope BZ-X800	Keyence
Critical Point Dryer CPD 030	Baltec
Cassette and Compact Slide Printer VCP 5001	VOGEL
Spin Tissue Processor Microm STP 120	Thermo Scientific™

Table 3.2 Chemicals for the syntheses and characterization methods

Chemicals	**Info (formula, concentration, components, purity)**	**Manufacturer**
Dulbecco's Phosphate Buffered Saline (PBS)	Without calcium chloride and magnesium chloride	Sigma Aldrich
Ethylenediaminetetraacetic acid (EDTA)		Sigma Aldrich
Trypsin		Invitrogen GmbH
Sodium Chloride	NaCl	Panreac AppliChem
Polyethylene Glycol (PEG)	$(C_2H_4O)_nH_2O$, average Mn 6000	Sigma Aldrich

Table 3.2 Chemicals for the syntheses and characterization methods (continued)

Paraffin		Sigma Aldrich
Entellan		Merck
Histofix Formaldehyde	Acid-free, 4% phosphate buffered formaldehyde solution	Carl Roth
Alizarin Red S		Morphisto
4′,6-diamidino-2-phenylindole (DAPI)		Sigma Aldrich
Paraformaldehyde (PFA)		Carl Roth
Ethanol	C_2H_6O, ≥ 99,8 % purity	Carl Roth
Hydrochloric Acid	HCl, 6 mol/L	Carl Roth
Polycaprolactone (PCL)	$(C_6H_{10}O_2)_n$	Sigma Aldrich
Trypan blue		Sigma Aldrich

Table 3.3 Chemicals for cell cultures

Chemicals	**Info (formula, concentration, components, purity)**	**Manufacturer**
Dulbecco's Modified Eagle Medium (DMEM) (1X) + GlutaMAXTM-1	[+] 4,5 g/L D-Glucose [-] Pyruvat	Gibco
Penicillin/streptomycin		Sigma Aldrich
Fetal calf serum (FCS)		PAN Biotech
Dexamethasone		Sigma Aldrich
Ascorbic acid 2-phosphate	8.3 mg/ml	Sigma Aldrich
ß-Glycerophosphate	1 M	Sigma Aldrich
Ethanol	C_2H_6O, ≥ 99,8 % purity	Carl Roth
Polyamide 6	$(–NH–(CH_2)_5–CO–)_n$	Carl Roth

Table 3.4 Cells with donor details

Cells	**Donor number**	**Usage**
Pre-osteoblast	SP1, P4, 1 million cells, 2013, (Pre-osteoblast donor 1)	CaP and EVs Obtaining
Pre-osteoblast	SP2, P4, 1 million cells, 2013, (Pre-osteoblast donor 2)	CaP and EVs Obtaining
Pre-osteoblast	SP3, P4, 1 million cells, 2013, (Pre-osteoblast donor 3)	CaP and EVs Obtaining

Table 3.5 Composition of media and solutions for cell cultures

Solution	**Composition**
Cell Growth Medium	DMEM 10% FCS 1% penicillin/streptomycin
Differentiation Medium	DMEM 10% FCS 1% penicillin/streptomycin 1 % ß-Glycerophosphate, 0.6 % ascorbic acid 2-phosphate, 0.01 % dexamethasone/ethanol 1:10 v/v

3.2 Instructions for Experimental Methodology

The following experimental steps were carried out to isolate EVs from osteoblast cells for use in biomimetic CaP production studies:

- A pre-experiment involving CaP NP production from osteoblast cells
- EVs were isolated from osteoblast cells using standard ultracentrifugation and PEG-precipitated ultracentrifugation methods.
- Isolated EVs were combined with synthetic collagen fibers to form gels.
- A collagen matrix was produced using isolated EVs, synthetic collagen fibers and osteoblast cells. This collagen matrix was used to manufacture a bone-like 3D bioprinted material.

In the following paragraphs, details will be provided for the above steps.

3.2.1 CaP NPs Synthesis

3.2.1.1 Cell Growth

The cell growth medium was warmed to 37°C for 15 minutes in a water bath. 9 mL of the heated medium was transferred to 3 different 50 mL centrifuge tubes. All 3 pre-osteoblast donor cells were removed from the -80°C freezer and placed separately in the 50 mL centrifuge tube with 9 mL of warmed medium. Frozen cells were thawed and suspended in by moving up and down with an Eppendorf pipette.

Cell suspensions were centrifuged at 300 g for 5 minutes. After centrifugation, the supernatants were removed, and 5 mL of warmed cell growth medium was added to each 50 mL centrifuge tube. Pellets were resuspended in the tube and transferred to 3 different 175 cm^2 tissue culture flasks. 10 mL of the warmed cell growth medium was added to each cell flask. Then the cells were incubated for 2 weeks at 37 °C. Cell media was changed 2 times per week during incubation. After 2 weeks of incubation, each cell donor was divided into 2 groups and seeded onto 2D well plates and 3D tissue scaffolds as illustrated in Figure 3.1.

3.2.1.2 Cell Seeding

The old cell medium was removed and 10 mL of trypsin-PBS-EDTA was added to the cell flasks to wash them. The cell flasks were incubated at 37 °C for 2 minutes and then transferred separately to centrifuge tubes. The cell solutions were centrifuged at 300g for 5 minutes at room temperature and the supernatants were removed. 2 mL of the differentiation medium was added to the pellets and the cells were resuspended by pipetting up and down. The cell concentrations were calculated using the cell counting chamber method (details are in section 3.3.1.1 Cell counting). Each cell sample was divided into 2 groups for seeding

3D Environment:

1 mL of PBS-EDTA was seeded to each well of a 12-well plate. 3D dimensional tissue scaffolds (electrospun polyamide 6 produced by Weigel and colleagues [58]) were inserted into a crown and placed in the well plates. Cells were added to the 3D tissue scaffolds and 1.5 mL of differentiation medium was added to each well.

2D Environment:

Cells were seeded to the 12-well plate. 1.5 ml of differentiation medium was added to each well. 3D and 2D scaffolds were placed in the incubator at 37°C.

3.2.1.3 CaP Production

After seeding, the cells were incubated with the differentiation medium at 37°C for 2 weeks. The differentiation medium was stored at 4°C. The medium was changed 3 times a week and the old medium was collected. The day the differentiation medium was started was considered as day 0. Each collected medium was labeled with the number of the day it was collected (day 2,5,7,9 etc). The collected media

were incubated at 37 °C for one week. After incubation, the media were washed with 0.5 mL of 0.9% NaCl and stored at -20 °C.

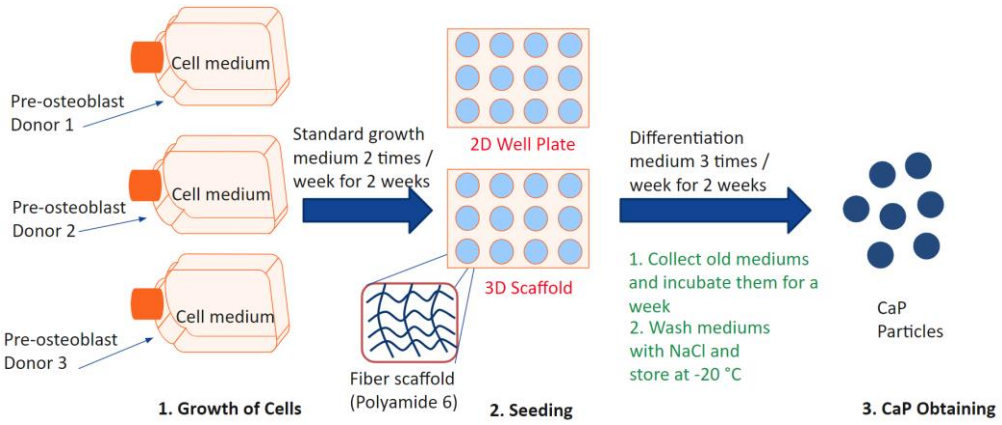


Figure 3.1 Schematic representation of the CaP production process

3.2.2 Extracellular Vesicle Obtaining

3.2.2.1 Cell Growth

The preosteoblast donor 1 cells were incubated in a cell flask as described above in "3.2.1.1 Cell Growth". The cell growth medium was changed twice a week during the incubation period.

3.2.2.2 EV Isolation

After 2 weeks of incubation, the cell growth medium was discarded, and 15 mL of the warmed differentiation medium was added to the cell flask. The cell flask was incubated at 37 °C for 4 weeks, with the cell medium changed 3 times a week. Old medium was transferred to a 50 mL centrifuge tube. The day the differentiation medium was started was considered as day 0. Each collected medium was labeled with the number of the day it was collected (day 2,5,7,9 etc). The collected media were divided into 2 parts for 2 different isolation methods. The isolation methods were set up based on the studies of Ludwig and colleagues [59].

In the first isolation method, as depicted in Figure 3.2a, EVs were isolated using the PEG-precipitated ultracentrifugation method [59]. The collected media were centrifuged at 10,000 g, 30 minutes. After centrifugation, the supernatants were transferred to another centrifuge tube. 0.85 mL of 10% PEG was added to the supernatants. After gently mixing, the solution was incubated overnight at 4 °C. The solution was centrifuged at 1500 g for 30 minutes at 4 °C. The pellets were

collected and washed with 7.5 ml of 0.9% NaCl. After washing with NaCl, the solution was centrifuged at 110,000 g, 2 hours, 4 °C using an ultracentrifuge. Pellets were collected and dissolved in 250 µL of 0.9% NaCl. The isolated medium was stored at -20 °C.

In the second isolation method, EVs were isolated by ultracentrifugation without PEG precipitation [59] (Figure 3.2b). The collected media were centrifuged at 10,000 g for 30 minutes at room temperature. After centrifugation, the supernatants were transferred to another centrifuge tube and ultracentrifuged at 110,000 g, 2 hours, 4 °C. The pellets were collected and washed with 7.5 ml of 0.9% NaCl. After washing with NaCl, the solution was ultracentrifuged at 110,000 g, 2 hours, 4 °C. The pellets were collected and dissolved in 250 µL of 0.9% NaCl. The isolated EVs were stored at -20 °C.

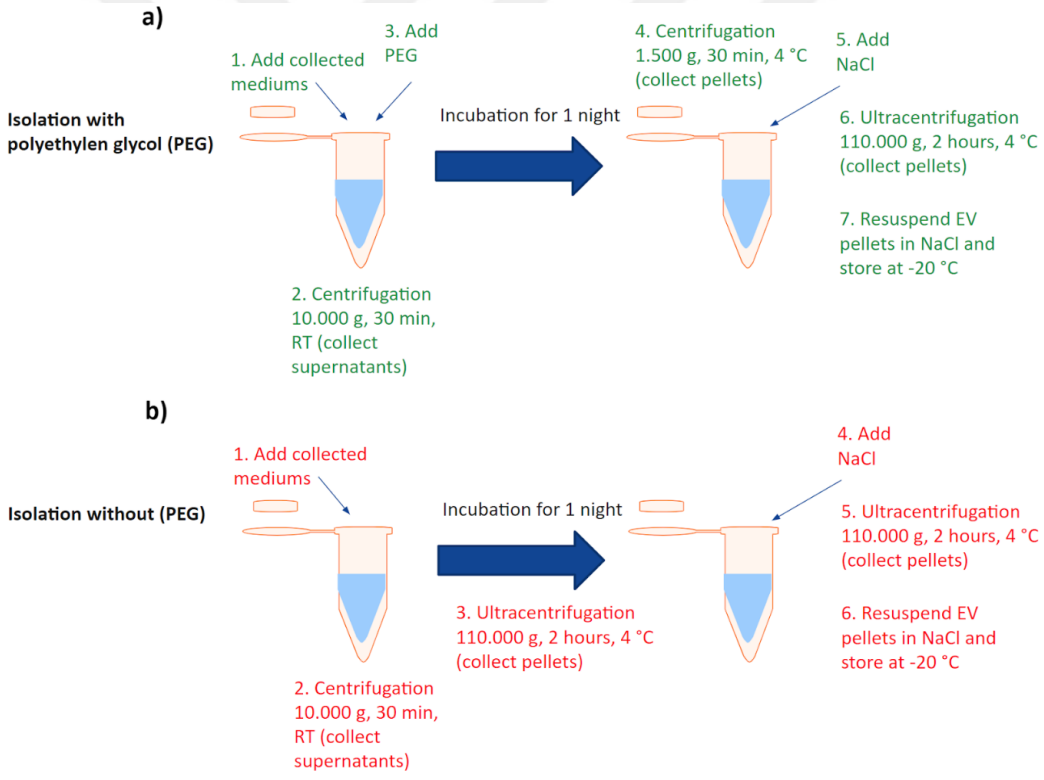


Figure 3.2 Schematic representation of EV isolation methods, **a:** Isolation with PEG, **b:** Isolation without PEG

3.2.3 Calcification EVs in Collagen Gels

2 different collagens were used for the calcification process of EVs. The first one is acidic collagen solutions from rat tail (we will call it standard collagen shortly) and the second one is printing collagen. Printing collagen is a special composite of

standard collagen and a polyanion. The role of the polyanion is to slow down the gelation process of the collagen by temporarily binding its peptides.

EVs were removed from the freezer and placed in an ice bucket. Printing collagen, standard collagen solution, gel neutralization solution (GNS) and differentiation medium were taken from the refrigerator. Differentiation medium was warmed at 37°C for 15 minutes.

Printing collagen gel production

20 mg of printing collagen was placed in a petri dish. It was then transferred to a 5 mL syringe. 450 µL of the differentiation medium and 200 µL of GNS were added to the syringe. The syringe was connected to another empty syringe. The materials were transferred to the other syringe by pushing the filled syringe. In this way, the materials were mixed by exchanging them between the two syringes. The second syringe was removed and 50 µL of PEG precipitated EVs was added to the filled syringe through the connector. The syringes were connected, and the samples were mixed between the syringes. The mixture in the syringe was centrifuged at 300 g for 20 seconds at room temperature. After centrifugation, air bubbles were partially removed, and the solution was mixed between syringes. The solution was added dropwise to a 12-well plate petri dish using a pointed syringe. The petri dish was placed in an incubator at 37°C. After 1 hour, the samples were gelled. 1 mL of differentiation medium was added to each well and the 12-well plate was incubated at 37°C for 2 weeks. The medium was changed once a week.

The same procedure was performed for EVs without PEG precipitation. As a result, 2 different gel groups were obtained: Printing collagen - EVs precipitated with PEG and printing collagen - EVs without PEG precipitation.

Standard collagen gel production

The same procedure was repeated for the standard collagen gel preparation. 1 mL of the standard collagen was used instead of printing collagen. 2 different groups of standard collagen gels were obtained: Standard collagen - EVs precipitated with PEG and Standard collagen - EVs without PEG precipitation.

A collagen gel with CaP NPs was also prepared for the control group. No EVs were used in this gel.

As summarized in Figure 3.3, 5 different gel groups were obtained as a result of the gelation process:

- Printing collagen - EVs precipitated with PEG.
- Printing collagen - EVs with no PEG precipitation.
- Printing collagen - CaP NPs
- Standard collagen - EVs precipitated with PEG.
- Standard collagen - EVs with no PEG precipitation.

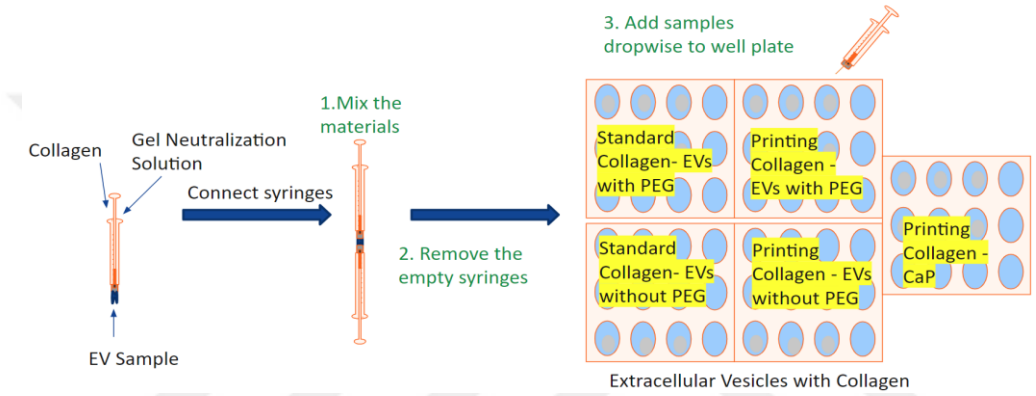


Figure 3.3 Schematic representation of the methodology of the preparation of 5 different types of collagen gels

3.2.3.1 Incubation and Finalization of Gels

As shown in Figure 3.4, the resulting gels were incubated with the differential medium to produce CaP. The gels were fixed after 2 weeks of incubation. They were removed from the incubator and the media were discarded. 1 mL of histofix formaldehyde was added to each gel. After the addition of histofix formaldehyde, the gels were left at RT for 2 hours. The histofix formaldehyde was then discarded and the gels were washed twice with 1 mL PBS. Then 1 mL PBS was added to the gels and the well plate was covered with paraffin. The washed gels were stored at 4°C.

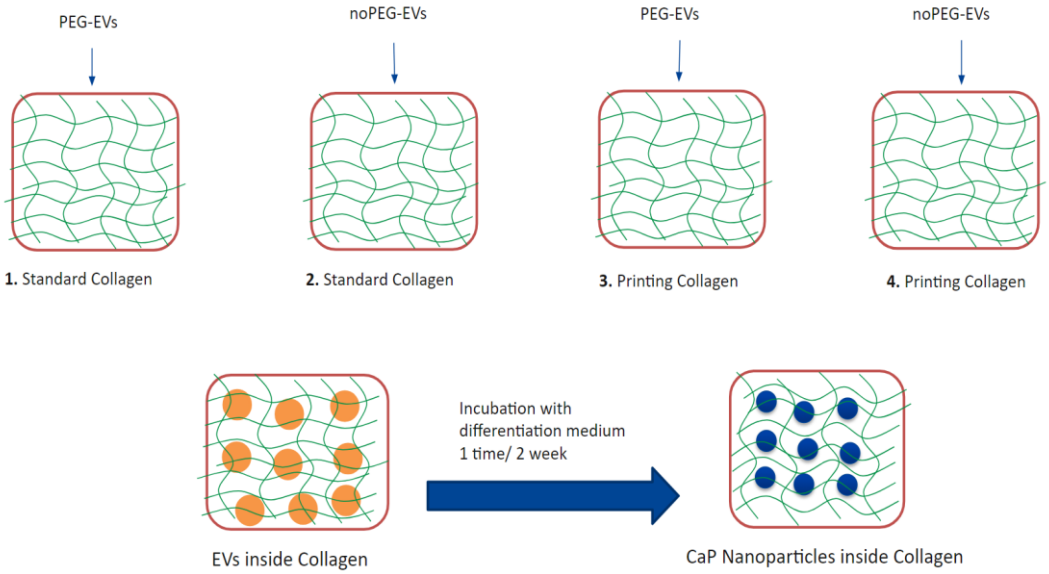


Figure 3.4 Schematic representation of 4 different ways of obtaining gels and CaP production from these gels

3.2.4 Calcification of Collagen-EVs-Cell Gels

Collagen gels were prepared using the same method described in the section "3.2.3. Calcification EVs in collagen gels". Additionally, CaP NPs and osteoblast cells were added to some gels. For that, osteoblast cells were also harvested by centrifugation at 300g for 5 minutes and suspended in 150 µL of differentiation medium. As a result of the gelation process, 8 different gel groups with 5.4 mg/ml final concentration were obtained:

- Standard collagen - EVs with no PEG precipitation.
- Standard collagen - EVs with no PEG precipitation - Osteoblast cells
- Standard collagen - CaP NPs
- Standard collagen - CaP NPs - Osteoblast cells
- Printing collagen - EVs with no PEG precipitation
- Printing collagen - EVs with no PEG precipitation - Osteoblast cells
- Printing collagen
- Standard collagen

3.2.4.1 Incubation and Finalization of Gels

Gels were incubated for 2 weeks, and the process was finalized as described at "3.2.3.1 Incubation and Finalization of Gels".

3.2.5 3D Bioprinting

The 3D bioprinting model was designed by the RegenHu Shaper software and printed by the R-GEN 200 Bioprinter. The bioprinting model was drawn using the R-GEN controller program. The model consisted of 4 components and 11 layers as given in Table 3.6.

Table 3.6 Components of 3D bioprinting model

Component	Material	Role	Number of layers
Frame	Polycaprolactone (PCL)	Shaping the biomaterial	4
Collagen matrix	Printing collagen GNS Osteoblast cells EVs Differentiation medium	Main component	4
Stabilization fiber	Polycaprolactone (PCL)	Providing mechanical support	2
Grill	Polycaprolactone (PCL)	Providing a biomimetic channel for fluid transport	1

EVs, printing collagen and GNS were removed from the freezer and placed in an ice bucket. Differentiation medium was warmed at 37°C for 15 minutes. Osteoblast cells were also isolated by centrifugation at 300 g for 5 minutes and suspended in 100 µL of differentiation medium. They were then counted using the cell counting chamber method as described earlier in section 3.3.1.1 cell counting.

The collagen matrix was prepared as described in the section "3.2.3. Calcification EVs in collagen gels", except for the incubation part to prevent gelation. 40 mg printing collagen, 200 µl GNS, 100 µl cell suspension, 250 µl EVs and 900 µl differentiation medium were used in the collagen matrix. The collagen matrix and PCL were transferred to 2 different printing slots. The collagen matrix was printed with the Bioprinter The R-GEN 200 which is shown in Figure 3.6 at 6 kPa, while 200 kPa was used for the PCL components. 2 biomaterials were produced using this method.

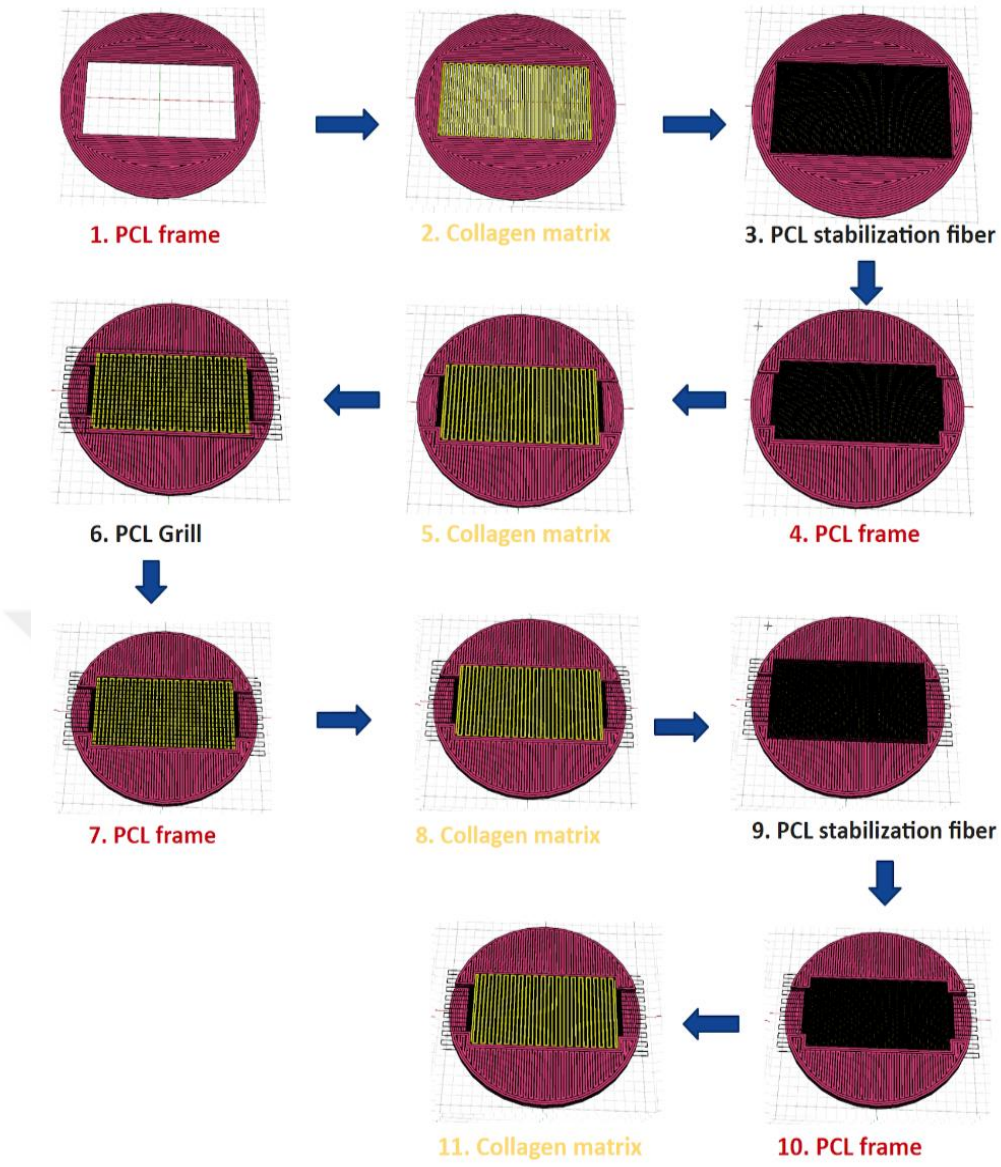


Figure 3.5 Schematic representation of the steps involved in the 3D bioprinting

The 3D bioprinted samples shown in Figure 3.7 were incubated at 37°C for 30 minutes, and then 5 mL of differentiation medium was added to the biomaterials. The bioprinted materials were incubated at 37°C for 4 weeks for the calcification process.



Figure 3.6 An image taken from the 3D bioprinting process

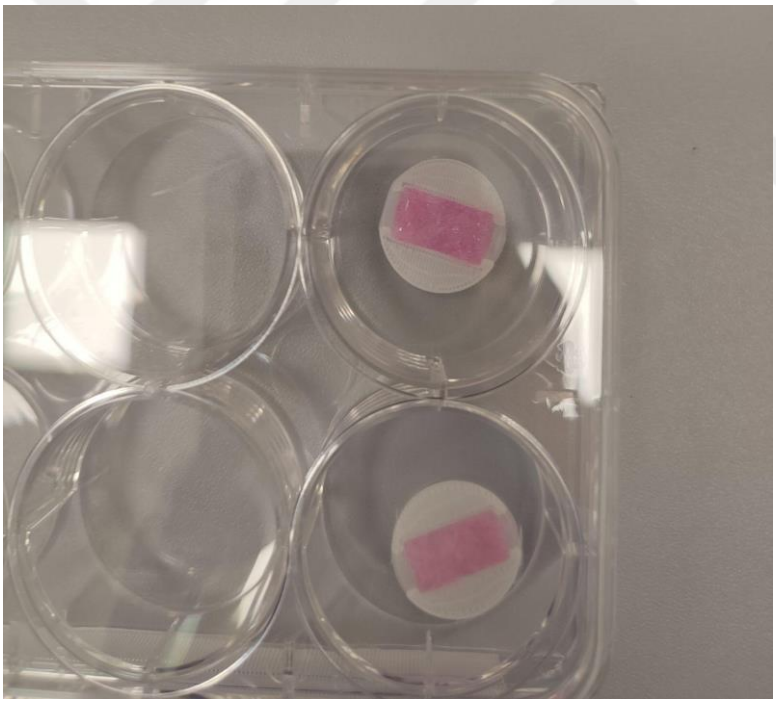


Figure 3.7 3D bioprinted samples

3.3 Characterization Methods

3.3.1 Cell Counting

After 2 weeks of incubation with standard growth medium, cells were counted using a Neubauer chamber. After washing with 10 ml PBS-EDTA, 7 mL of the standard

growth medium was added to the cells. Cells were then isolated by centrifugation at 300 g for 5 minutes at RT. Cells were resuspended in 100 µl of standard growth medium. 10 µl of cell suspension was mixed with 90 µl of trypan blue and added to the counting chamber. The number of dots in each square was counted and averaged under the Leica DMi 1 cell culture microscope. The cell concentration (cells/ml) of each cell was determined using the equation (3.1).

$$Cell\ density\ \left(\frac{cells}{mL}\right) = (Average\ number\ of\ cells\ counted) \times (Dilution\ factor) \times\ 10^4 \quad (3.1)$$

3.3.2 ICP-MS

CaP NPs, EVs and collagen gels were analyzed by inductively coupled plasma mass spectrometry (Thermo Fisher Scientific - ICP-MS, iCAP RQ) to determine their Ca and P ion content. CaP NPs and EVs were dissolved in 300 µl of pure water, while collagen gel samples were dissolved in 6 N hydrochloric acid solution (0.5 mL) for 6 h at 95 °C. Samples were diluted in extra pure water (1:100). Each sample was measured 3 times, and the average concentrations were calculated. Ca and P ions were measured based on 1000 mg/L standards.

3.3.3 NTA

The concentration and average size of CaP NPs and EVs that dissolved in 0.9 % NaCl were characterized using the ZetaView® basic NTA-PMX-120 nanoparticle tracking analyzer (NTA). All samples were diluted in bi-destilled water (1:10) and analyzed using the following parameters: sensitivity: 60, shutter: 150 and frame rate: 15.

3.3.4 Staining with Alizarin Red and DAPI

The cells (after incubation with the differentiation medium for 2 weeks), the collagen gels and the bioprinted materials were stained with alizarin red to detect adherent CaP and with 4′,6-diamidino-2-phenylindole (DAPI) to demonstrate the presence of cells by detecting their nuclei. 1 mL of 4% paraformaldehyde (PFA) was added to each sample. Samples were stored at 4 °C overnight. The samples were then washed twice with pure water and 0.3 mL of alizarin red dye was added. After 2 minutes, the samples were washed with water and 0.3 mL of DAPI was added to each well plate. After 2 minutes, the DAPI was removed, and the samples

were washed with water. Images of the samples were taken at 10X or 20X magnification to show CaP NPs and cell nuclei (OP-87762 filter from Keyence) using a fluorescence microscope.

3.3.5 TEM

The structure and size of CaP NPs and EVs were characterized by transmission electron microscopy (TEM). Samples were suspended in 10 µl of water and placed on copper grids coated with 200 mesh carbon (Sigma Aldrich). After placement, the copper grids were allowed to dry at room temperature for 5 min. The samples were then analyzed using a JEOL - JEM2100 analytical electron microscope at 200 kV.

3.3.6 SEM

Scanning electron microscopy (SEM) was used to determine the size and surface morphology of the collagen-EVs-cell gels. Samples were dried by using a Baltec CPD 030 critical point dryer. The samples were placed on conductive carbon pads. Then, they were sputtered with platinum for 25 seconds at 30 mA with 9 cm distance by using the Balzer Union - MED010 sputtering device. SEM images were taken by using Zeiss - Supra 25 SEM micrograph. An SE2 detector was used with 1.5 kV accelerating voltage. The elemental composition of samples was analyzed by energy dispersive X-Ray analysis (EDX) with following parameters: voltage: 10 kV, wide: 8.5 mm. The SE2 detector was used also for EDX analysis.

4
RESULTS AND DISCUSSION

The objective of this study was to isolate EVs from osteoblast cells for biomimetic CaP production. Initially, pre-osteoblasts were cultured in standard medium to develop into osteoblasts. EVs were then isolated from these osteoblast cells using both standard ultracentrifugation and PEG-precipitated ultracentrifugation methods. These isolated EVs were mixed with synthetic collagen fibers to form gels, which were incubated with differentiation medium to produce CaP NPs. Furthermore, a collagen matrix incorporating the isolated EVs, synthetic collagen fibers, and osteoblast cells was created and utilized to produce a bone-like 3D bioprinted material. The study examined CaP production and the cell viability of this 3D bioprinted material after a three-week incubation with differentiation medium. The results of these processes will be presented and discussed in the following sections.

4.1 CaP NPs Obtaining

4.1.1 Results of Synthesis Process

A pre-experiment was designed to test the CaP production of preosteoblast cells. CaP NPs were synthesized from 3 different preosteoblast donor cells. In this context, 2 different seeding methods were used to compare their effect on CaP production: 2D and 3D environment. Since osteoblast cells bind to collagen fibers and produce CaP NPs in a 3D environment during the physical mineralization process, an artificial 3D environment made up of polyamide 6 was therefore used to see the effect on the productivity of CaP production. Pre-osteoblast cells were incubated for 2 weeks to grow and transform into osteoblast cells. Light microscopy images of each donor cell were taken at the end of the first and second week of incubation. The cell concentration of each donor was calculated by the cell counting chamber method at the end of the second week.

According to the light microscopy images illustrated in Figure 4.1, preosteoblast donor 1 cells have the most intense cell morphology at the end of both the first and second week. On the other hand, pre-osteoblast donor 2 cells have the least intense

cell morphology, meaning that their proliferation and osteogenic differentiation ability was the lowest among all donors.

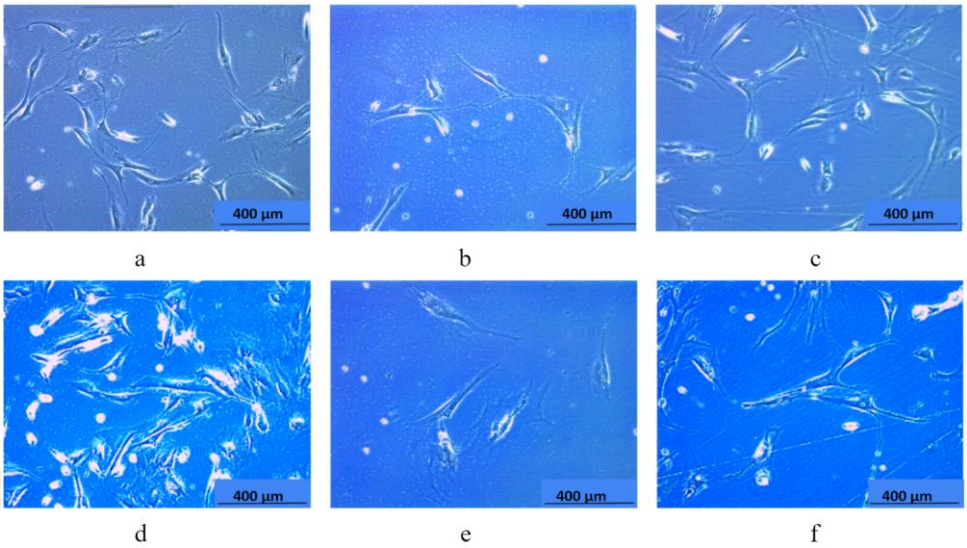


Figure 4.1 Light microscopy images of preosteoblast cells after 1 week (a – c) and 2 weeks (d – f) of incubation at 10X magnification, **a:** Preosteoblast donor 1, **b:** Preosteoblast donor 2, **c:** Preosteoblast donor 3, **d:** Preosteoblast donor 1, **e:** Preosteoblast donor 2, **f:** Preosteoblast donor 3

The cell counting results given in Table 4.1 also showed that osteoblast donor 1 has the highest cell concentration with 615000 cells/mL, followed by donor 3 (390000 cell/mL), while osteoblast donor 2 had the lowest concentration result with 220000 cells/mL. Although all 3 donors were incubated under the same conditions, visible differences in cell proliferation were observed due to factors such as general donor variation and donor medical history.

After 2 weeks of incubation, each donor of cells was divided into 2 material structure groups (2D and 3D) for osteogenic differentiation and CaP production.

4.1.2 Characterization Results of the CaP NPs

The presence of Ca and P ions in CaP NPs obtained from 3 different donors with 3D environment was determined by ICP-MS as shown in Table 4.1 where the Ca/P ratios were also calculated from the ion concentration data. The Ca/P ratios obtained from different samples of donor 2 and donor 3 were between 1.07 and 1.31, indicating that they were in the brushite form [60]. On the other hand, the ratio was 1.61 in the sample obtained from donor 1, which is very close to 1.67 (Ca/P ratio of HA form [60]). It is thought that donor-related factors, such as the general donor

variation and donor medical history mentioned above, may have caused proportional differences, albeit small ones.

Table 4.1 Ca/P ratio of samples obtained from 3D environment

Sample Name	**Ca/P Ratio**	**Form**
Donor 1, day 10	1.61	HA
Donor 2, day 3	1.07	Brushite
Donor 2, day 10	1.21	Brushite
Donor 3, day 3	1.24	Brushite
Donor 3, day 10	1.31	Brushite
Donor 3, day 14	1.24	Brushite

The Ca/P ion ratio of donor 1 samples obtained by 2D was also calculated from the ICP-MS data and the results are given in Table 4.2. The Ca/P ratio was found to be between 1.19 and 1.30 (brushite form) in the study conducted on samples taken on 3 different days. As the results here are close to the ratio of the samples obtained with the 3D environment, it has been concluded that the use of either 2D or 3D environment does not significantly affect the Ca/P ratio. One of the conclusions that can be drawn is that this ratio does not change proportionally with time. Due to the small received amount of CaP by cells, it was not possible to confirm the crystal structure with x-ray diffraction. Therefore, for further investigations the production of CaP has to be repeated on a higher scale.

Table 4.2 Ca/P ratio of donor 1 samples obtained from 2D environment

Sample Name	**Ca/P Ratio**	**Form**
Donor 1, day 3	1.30	Brushite
Donor 1, day 10	1.27	Brushite
Donor 1, day 14	1.19	Brushite

The concentration and mean size of the CaP NPs produced were calculated by NTA. The concentration results are shown in Figure 4.2, while the mean size values are shown in Figure 4.3. The average concentration values are $2.72 \times 10^9 \pm 2.6 \times 10^8$ particles/mL and $3.49 \times 10^9 \pm 8.2 \times 10^8$ particles/mL for 2D and 3D environments, respectively. It seemed that there was no significant difference between the total NPs production of 2D and 3D environments. One reason for this situation might be that some of the CaP NPs produced in the 3D environment get stuck in the polyamide 6 scaffold and cannot get out into the medium. Also, the average mean size of the 2D and 3D environments was almost the same for each donor (198.9 ± 15.2 nm, and 198.8 ± 9.1 nm average mean sizes for 3D and 2D, respectively).

In reviewing the previous studies on CaP production, although some studies [61] have obtained CaP NPs with sizes close to 100 nm, most studies [62, 63, 64] have found that their sizes are generally around 50 nm. Although the reason why the NP sizes obtained in our study are much larger than those in the literature is not clearly known, it is thought that differences in the cell type and production techniques used may cause this.

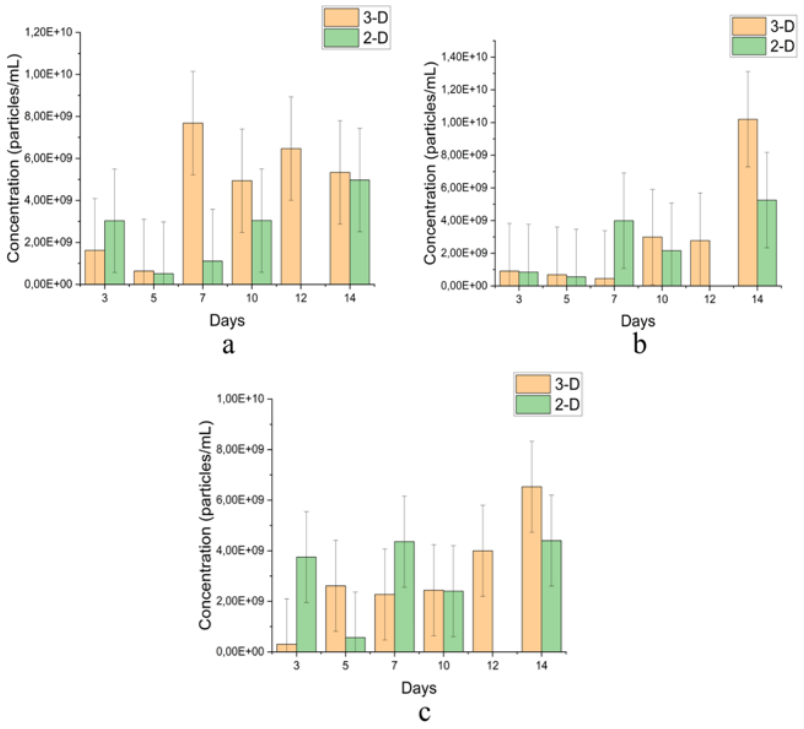


Figure 4.2 Concentration (particles/mL) results of CaP NPs obtained with NTA, a: 2-D and 3-D seeding of donor 1, b: 2-D and 3-D seeding of donor 2, c: 2-D and 3-D seeding of donor 3

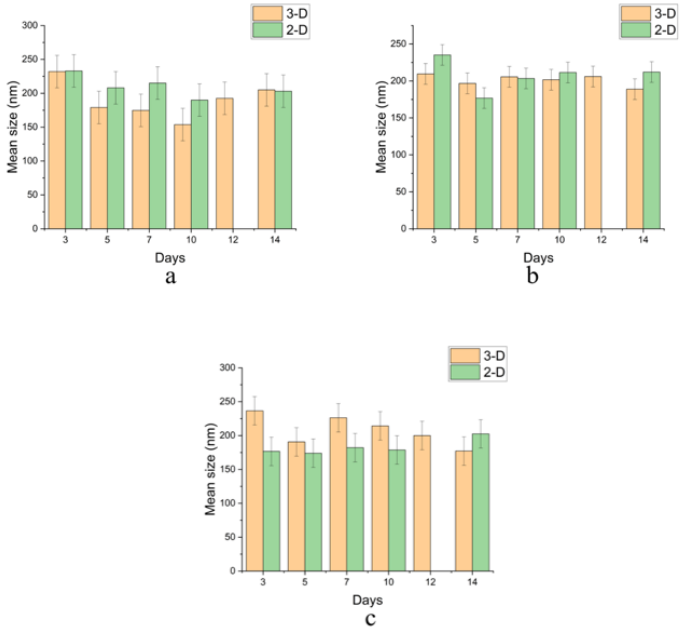


Figure 4.3 Mean size (nm) results of CaP NPs obtained with NTA, a: 2-D and 3-D seeding of donor 1, b: 2-D and 3-D seeding of donor 2, c: 2-D and 3-D seeding of donor 3

After CaP production was finished, the cells were stained with alizarin red and examined under a light microscope to detect the CaP NPs that did not enter the

medium. A strong red staining is observed for donor 1 (Figure 4.4.a) and donor 2 (Figure 4.4.b) for the 3D environment which indicates that a significant amount of CaP NPs still remains in the scaffold. Almost no CaP was observed by using donor 3 as shown in Figure 4.4.c.

For the 2D environment, a staining is observed for donor 1(Figure 4.4.d), but there is almost no red staining in case of donor 2 (Figure 4.4.e) and donor 3 (Figure 4.4.f). The reason for the observation of more NPs in the 3D environment can be explained by the stuck of NPs in the 3D scaffold. This situation could also explain why the average concentration differences were about 20% between 2D and 3D in the NTA results.

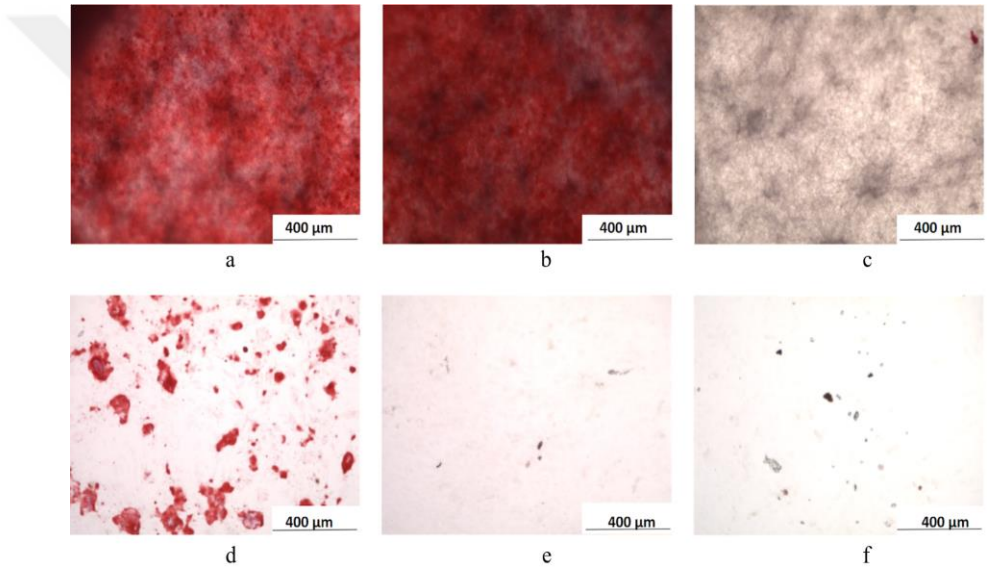


Figure 4.4 Light microscope images of osteoblast cells at 10X magnification after staining with alizarin red, **a:** Osteoblast donor 1 in 3D environment, **b:** Osteoblast donor 2 in 3D environment. **c:** Osteoblast donor 3 in 3D environment, **d:** Osteoblast donor 1 in 2D environment, **e:** Osteoblast donor 2 in 2D environment, **f:** Osteoblast donor 3 in 2D environment

Cells were stained with DAPI and examined by light microscopy to demonstrate the presence of cells by detecting their nuclei. According to the light microscopy images illustrated in Figure 4.5, a high DAPI staining is obtained for donor 1 and donor 3 in both 3D and 2D environments. For donor 2, almost no staining was observed in the 2D environment because the cells of donor 2 were not able to grow and proliferate sufficiently in this environment.

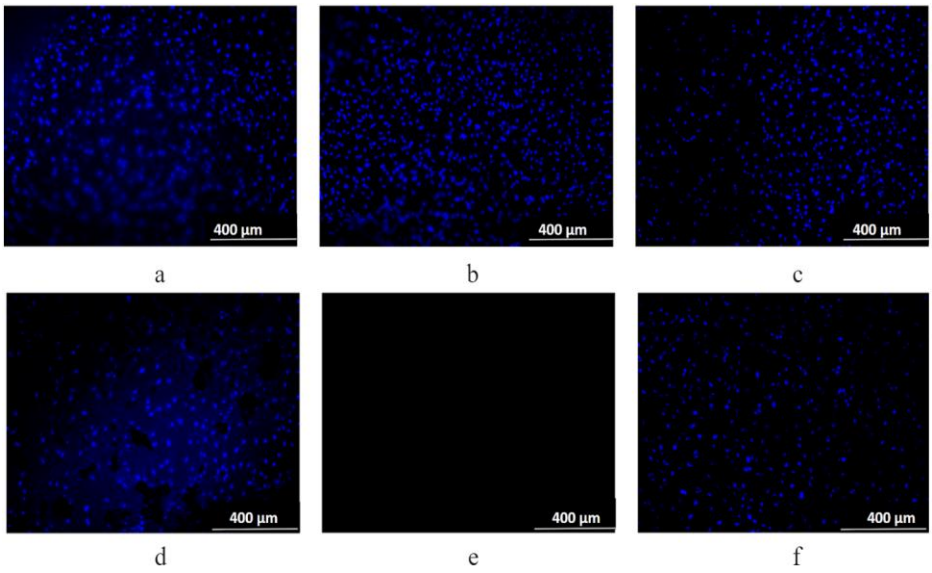


Figure 4.5 Light microscope images of osteoblast cells at 10X magnification after staining with DAPI, **a:** Osteoblast donor 1 in 3D environment, **b:** Osteoblast donor 2 in 3D environment, **c:** Osteoblast donor 3 in 3D environment, **d:** Osteoblast donor 1 in 2D environment, **e:** Osteoblast donor 2 in 2D environment, **f:** Osteoblast donor 3 in 2D

TEM was used to characterize the size and morphology of CaP NPs. The TEM images and the size distribution of the NPs are shown in Figure 4.6 and in Table 4.3, respectively. As a result, using samples obtained from donor 2 and donor 3 in 3D culture, almost all the NPs obtained were in spherical shape. On the other hand, NPs obtained at day 14 from donor 2 were in nanorod shape. The spherical particles show a wide size distribution between 65 nm and 300 nm, while the nanorod particles were slightly larger in size (94 - 390 nm).

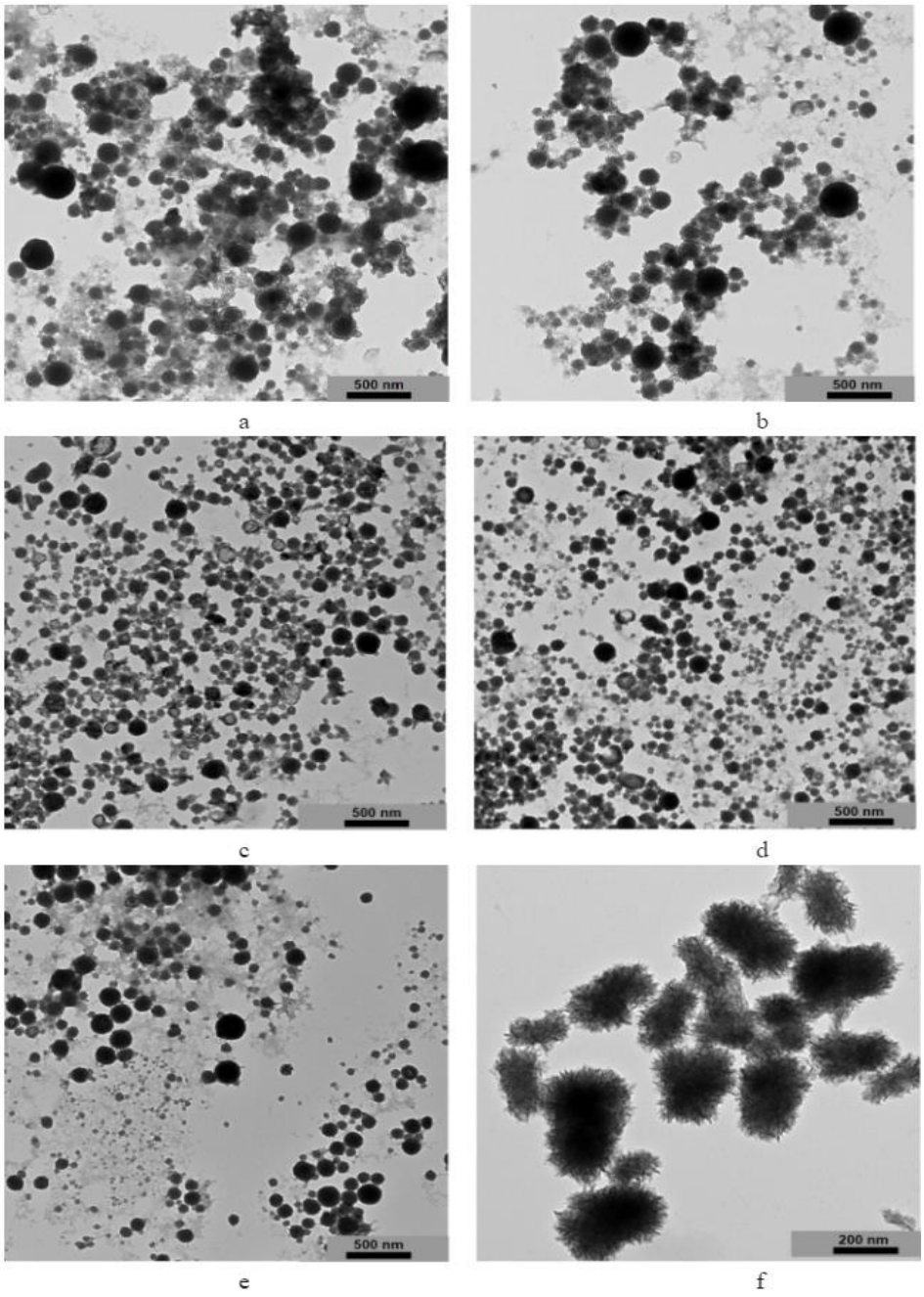


Figure 4.6 TEM images of CaP NPs obtained in 3D environment at day 3 (a-b), day 10(c-d) and day 14(e-f), **a:** Preosteoblast donor 2, **b:** Preosteoblast donor 3, **c:** Preosteoblast donor 2, **d:** Preosteoblast donor 3, **e:** Preosteoblast donor 3, **f:** Preosteoblast donor 2

Table 4.3 Size distribution of CaP NPs obtained in 3D environment

	Day 3	**Day 10**	**Day 14**
Donor 2	85.7 - 300 nm	42 - 121 nm	94-390 nm
Donor 3	68.8 - 263 nm	56 - 147 nm	65 - 251 nm

For the results shown in Figure 4.7 and Table 4.4 of TEM performed on 2D environments with donor 1 samples from different days, NPs obtained from day 14 were spherical with diameter values between 49.6 nm and 197.2 nm. It was observed that some NPs obtained from day 7 were in spherical form, while some of them were in nanorod form. On the other hand, NPs obtained on day 3 and day 10 were in agglomeration of nanorod form with diameter values between 114.9 nm and 490 nm. It was concluded that CaP NPs obtained in the 3D environment were generally in spherical form, while the samples obtained in the 2D environment were in both nanorod and spherical forms depending on the day. Although it is observed that the CaP shapes move from the nanorod form to the spherical form in the period from day 3 to day 14, the fact that it is densely in the nanorod form on day 10 prevents us from generalizing that the CaP shape changes proportionally to a spherical form over time.

In the NTA results, CaP NPs varied in a narrow size range between 182 nm and 209 nm, whereas in the TEM results, the particle sizes varied in a much wider range between 42 nm and 490 nm. Here, NTA measurements show only average dimensions, hence the narrower range. The fact that the majority of particles in the TEM results are between 150 nm and 250 nm can be interpreted as similar NP sizes being obtained by two different methods.

Investigating the TEM results of previous CaP production studies, it can be seen that in some studies [61, 63] the NPs are almost completely round and have a particle size varying between 30-100 nm. In some studies [62, 64], round particles of about 50 nm and nanorods of about 80 nm have been found. Although our study is very similar to studies in the literature in terms of NP shape, it is noteworthy that the particle sizes are much larger than in previous studies. Although the reason for

the difference in NP size is not fully known, it is thought that the main factor may be the difference in cell types and production techniques used, as mentioned above.

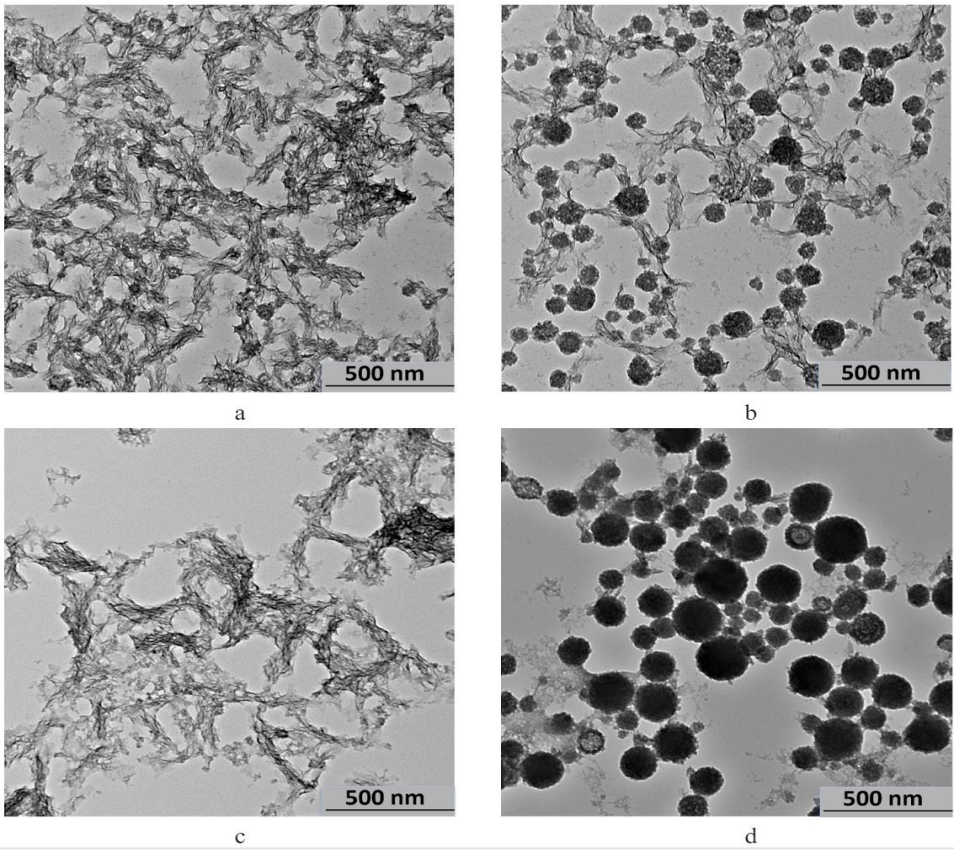


Figure 4.7 TEM images of the CaP NPs obtained from preosteoblast donor 1 in 2D environment, **a:** Sample obtained on day 3, **b:** Sample obtained on day 7, **c:** Sample obtained on day 10, **d:** Sample obtained on day 14

Table 4.4 Size distribution of CaP NPs obtained in 2D environment from osteoblast cells

	Day 3	**Day 7**	**Day 10**	**Day 14**
Donor 1	135 - 284 nm	49.6 -135nm	114.9 - 490 nm	49.6 - 197.2 nm

As a result of all the characterization processes, it was concluded that

Donor 1 had the best cell observation and concentration. The CaP concentration values are also higher than the other donors.

More CaP NPs were produced in the 3D environment compared to the 2D environment based on the Alizarin Red staining shown in Figure 4.4. However,

because some of the NPs were stuck at the 3D scaffold, the concentration values of the collected CaP NPs were almost the same. Therefore, the 2D environment is considered more advantageous than the 3D environment because it was easier to work with.

As a result, the 2D environment and donor 1 were chosen for the next experiments.

4.2 Results of EVs Isolation

Since PEG is widely used to increase the precipitation of vesicles by decreasing their solubility in water, the efficiency of PEG precipitation was investigated. Preosteoblast cells were incubated, and old mediums were collected as described at pre-experiment setup. Then EVs were isolated from the collected mediums using both PEG precipitation and no-PEG precipitation methods.

The concentration and mean size of the EVs produced were calculated by NTA. The concentration results are shown in Figure 4.8a while the mean sizes are given in Figure 4.8b. The average concentration values of EVs isolated with and without PEG were $2.3 \times 10^{10} \pm 2 \times 10^{10}$ particles/mL and $1.2 \times 10^{10} \pm 1.8 \times 10^{10}$ particles/mL, respectively. There was 91% difference between EVs produced with PEG precipitation and those produced without PEG precipitation. On the other hand, the mean sizes of EVs obtained with and without PEG methods were similar. The mean sizes of the PEG precipitation and no-PEG precipitation methods were 215 ± 35 nm and 240 ± 32 nm, respectively.

It is believed that the reason why more EVs were obtained using the PEG precipitation technique compared to the no-PEG precipitation technique is due to the precipitation effect of PEG molecules on EVs, as stated in the study conducted by Ludwig and colleagues [59]**.** As seen in Table 4.8a, related studies [59, 65, 66] also confirm the effect of the presence of PEG on the obtained EVs concentration.

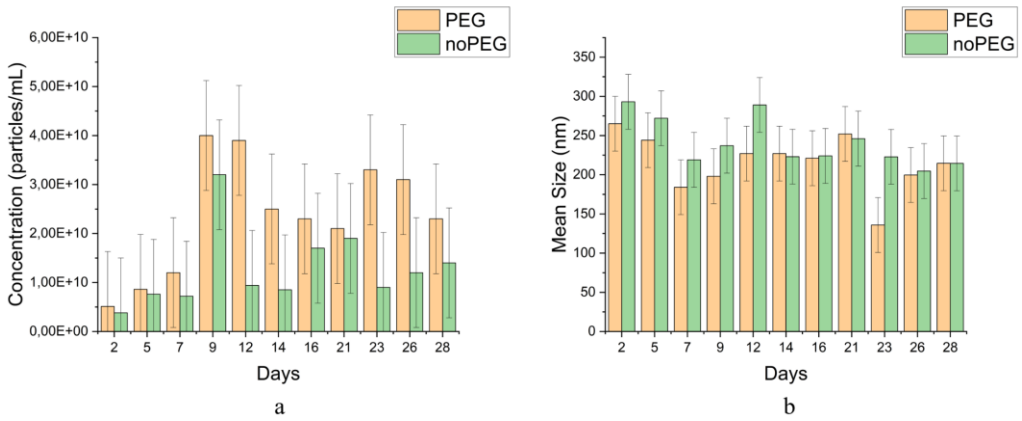


Figure 4.8 NTA results of EVs obtained with and without PEG precipitation, **a:** Concentration (particles/mL) results of EV samples, **b:** Mean size (nm) results of EV samples

ICP-MS was used to detect the presence of Ca and P ions in the EVs in order to check that EVs were obtained before converting into CaP. A highly concentrated CaP sample was also used in measurement as a control group. As depicted in Figure 4.9, no Ca and P ions were found in the EVs samples, which is an indication that the EVs were isolated before converted to CaP [16].

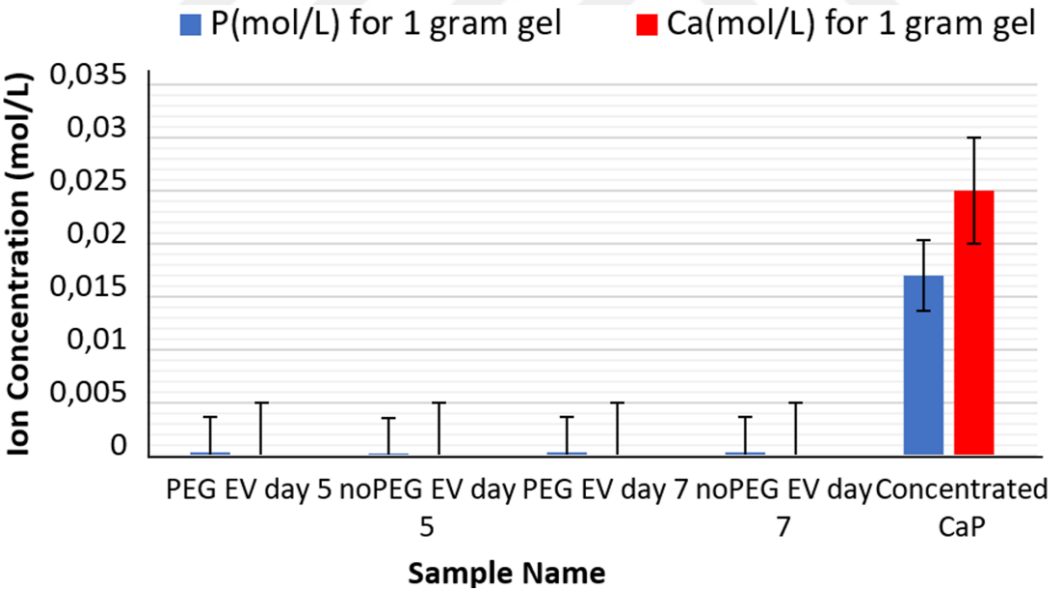


Figure 4.9 ICP-MS results showing the Ca and P ions content of EV and concentrated CaP samples

Summarizing the studies on EV isolation using different methods, it has been observed that the concentration values of EVs obtained are mostly between 10^8 and 10^{10} particles/mL. In this context, it can be said that the EV concentration values of 2.3×10^{10} particles/mL (with PEG) and 1.2×10^{10} (without PEG) particles/mL

obtained in this study were similar or even higher compared to the literature given in Table 4.5. Moreover, according to the study performed with the same method (PEG precipitation) using mesenchymal stem cells from which osteoblasts are derived [19], the concentration of EVs obtained in our study was approximately 10 times higher. In addition to the differences in cell type and cell culture used, it is thought that the difference in PEG incubation time and ultracentrifugation parameters may have caused the concentration difference between the two studies.

Studies of EV isolation from plasma cells using different techniques [65] concluded that the PEG precipitation technique was more effective than the ultracentrifugation and SEC techniques in obtaining higher concentrations of the EVs. While the concentration of EVs obtained by PEG precipitation was 1.27×10^{10} particles/mL, these data were measured as 8.24×10^{6} and 4.03×10^{9} for ultracentrifugation and SEC, respectively. Studies that focused on EV isolation from rat plasma [66], HEK293T cells [59], and THP-1 human monocytic cell line [67] also indicate that PEG precipitation is more effective in isolating EV compared to other methods.

It has been observed that the average size of EVs obtained from studies in the literature is mostly around 150 nm [59]. Considering that the average size of exosomes varies between 30 and 120 nm and the average size of microvesicles varies between 100 and 1000 nm, it can be concluded that the EVs obtained in these studies are exosome-microvesicle mixtures. Although the average EV sizes of 215 nm (PEG) and 240 nm (no-PEG) obtained in this study are above average, considering the 253 nm EVs isolated from plasma cells [65], it can still be concluded that they are an exosome-microvesicle mixture.

Table 4.5 EV isolation studies in the literature

Cell used in isolation	**Isolation Method**	**Concentration (particle/mL)**	**Average Mean Size (nm)**	**Reference**
Mesenchymal stem/stromal cells (MSCs)	PEG precipitation	2.0×10^9	100.3	[19]
THP-1 human monocytic cell line	Size exclusion chromatography	1.9×10^{10}	116.4	[67]
THP-1 human monocytic cell line	PEG precipitation	10^{12}	116	[67]
Mesenchymal stem cells (MSCs)	Size exclusion chromatography	no data	162.8	[20]
HEK293T	Ultracentrifuge	6×10^8	150	[59]
HEK293T	PEG precipitation (M.W: 6000)	8×10^8	140	[59]
HEK293T	PEG precipitation (M.W: 8000)	7×10^8	155	[59]
Human plasma	Ultracentrifuge	8.24×10^6	253	[65]
Human plasma	PEG precipitation	1.27×10^{10}	50	[65]
Human plasma	Size exclusion chromatography	4.03×10^9	49	[65]
Rat plasma	Ultracentrifuge	4.17×10^8	150	[66]
Rat plasma	PEG	5.43×10^{10}	130	[66]

4.3 Calcification of Extracellular Vesicles

After the production of EVs with and without the PEG method, gels were formed by combining both EV groups with 2 different collagens which are standard collagen and printing collagen. The purpose was to evaluate the CaP production potential of the different combinations: Printing collagen- EVs with PEG, printing collagen-EVs without PEG, standard collagen-EVs with PEG, and standard collagen-EVs without PEG. Printing collagen-CaP gel was also prepared for the control group.

After 2 weeks of incubation, the gels were stained with alizarin red as shown in Figure 4.10 to observe the CaP NPs produced. It was observed with the bare eye that the printing collagen-EVs without PEG gel and the standard collagen-EVs without PEG gel were darker in color, indicating more CaP

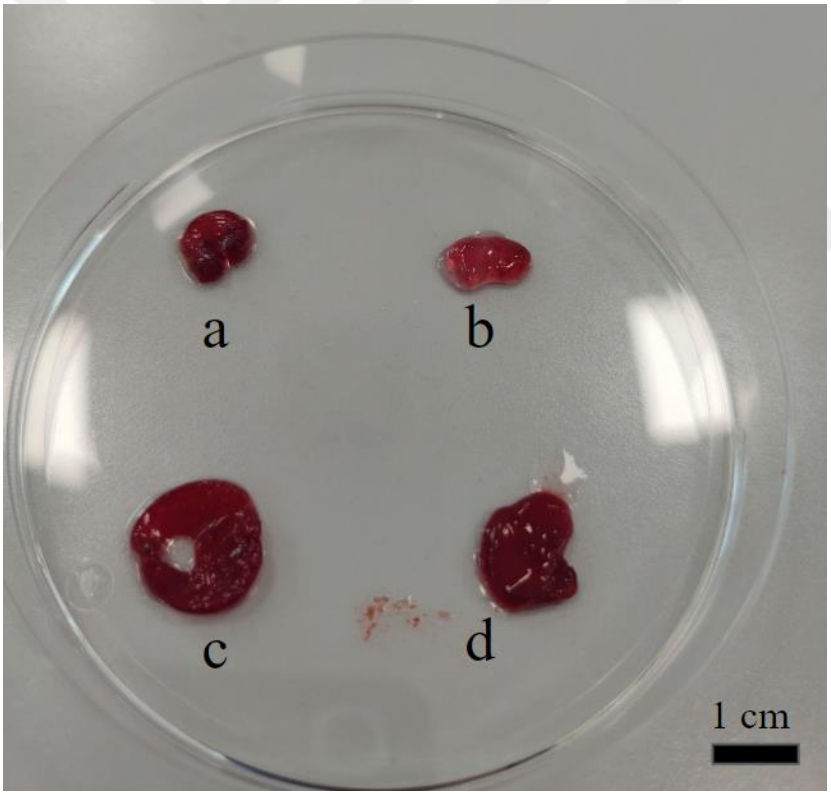


Figure 4.10 Images of collagen-EV gels after staining with alizarin red, **a:** Printing collagen-PEG EVs gels, **b:** Standard collagen-PEG EVs gel, **c:** Printing collagen-noPEG EVs gels, **d:** Standard collagen-noPEG EVs gel

For detailed observation, a cross section was taken from each gel and stained with alizarin red. They were then examined under a light microscope to detect the CaP

NPs produced. According to results shown in Figure 4.11, the CaP observation is the lowest for standard collagen-EVs with PEG and printing collagen-EVs with noPEG gels. Although the CaP observation is relatively higher for printing collagen-EVs with PEG gels on images, most of the particles are accumulated in a certain region and observations are not made outside this region. Therefore, it was concluded that standard collagen EVs without PEG showed the best CaP observation. It is thought that this situation arises due to the possibility that EVs produced by PEG precipitation contain some PEG residues even though they were washed with NaCl solution to remove the residues during the isolation process.

Since these PEG residues interact with vesicles by surrounding them [43]**,** they may have prevented the EVs from binding to the collagen fibers. It is believed that this situation makes it difficult for the EVs to bind to collagens, reducing their effectiveness and thus negatively affecting the production of CaP NPs.

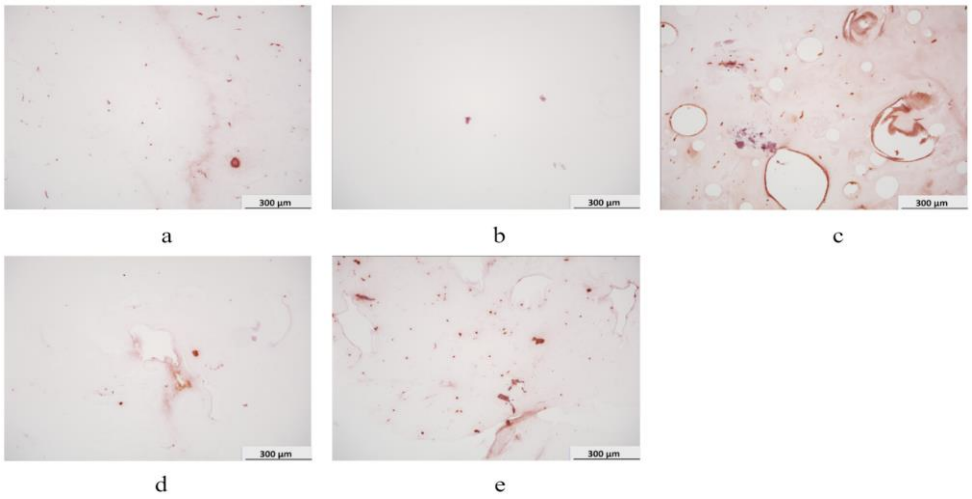


Figure 4.11 Light microscope images of collagen-EVs gel slides at 10X magnification after staining with alizarin red, **a:** Standard collagen-noPEG EVs gel, **b:** Standard collagen-PEG EVs gel, **c:** Printing collagen-CaP NP gels, **d:** Printing collagen-noPEG EVs, **e:** Printing collagen-noPEG EVs

After 2 weeks and 4 weeks of incubation, ICP-MS was used to detect the presence of Ca and P ions in the gels. The concentrations of Ca and P ions produced by the gels were also compared using the ICP-MS results shown in Figure 4.12. In parallel with the alizarin red staining results, standard collagen-EVs with PEG gel resulted in the highest Ca and P ion concentration at both 2 and 4 weeks. In addition, it seems like there was an increase in the production of Ca and P ions as the incubation

time of all the gels was increased. In the relevant study by Meng Zhao and colleagues [68], the opposite situation to our study was observed. CaP production was found to decrease after day 16. It is thought that the main difference is due to the different experimental and incubation conditions and environments.

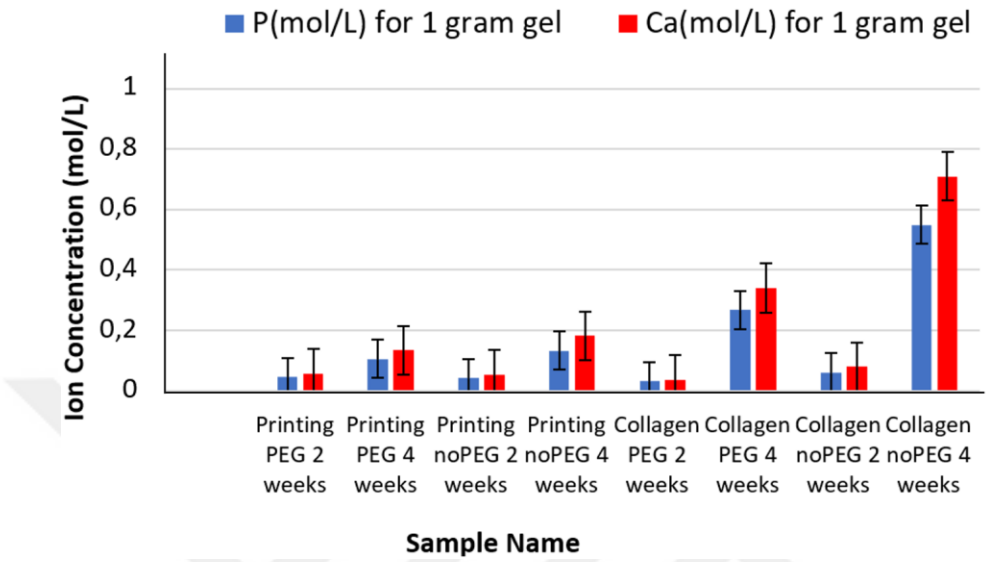


Figure 4.12 P and Ca ion concentration (mol/L) results of calcified gels obtained by ICP-MS after 2 weeks and 4 weeks incubations

Both alizarin red staining and ICP-MS results show that gels combined with PEG-precipitated EVs produce fewer CaP NPs.

4.4 Calcification of Collagen-EV-cell-gels

Since osteoblast cells play an important role in CaP production by secreting EVs [16], they were added to the gels to see their effect on CaP production when interacting with collagen including EVs. After 2 weeks of incubation, the presence of Ca and P ions was detected by ICP-MS as shown in Figure 4.13. The results show that all samples with cells produced significantly more CaP than the samples without cells. It is believed that the main reason for this is that the cells added to the gels produce EVs (and therefore CaP NPs [16]) during incubation, which increases the amount of CaP NPs produced by the gels. Among the gels with cells, the highest ion concentration was observed in the standard collagen-CaP NPs-cell gel samples, while the lowest concentration was observed in the collagen-noPEG EVs-cell gel samples. The printing collagen-noPEG EVs-cell gel samples had the second highest ion concentration values.

In contrast to the previous gel study, almost no Ca and P ions were found in printing collagen-noPEG EVs gels as well as in standard collagen-noPEG EVs gels. The EVs used in these gels were ultracentrifuged 3 times at 110000g for 2 hours during the isolation and concentration processes (2 times for isolation and 1 time for concentration). It is believed that the EVs may have been damaged and lost their CaP production function as a result of these high-speed rotations.

No Ca ion was found in the standard collagen gel and printing collagen gel samples since these gels did not contain EVs or osteoblast cells that would provide CaP production [16].

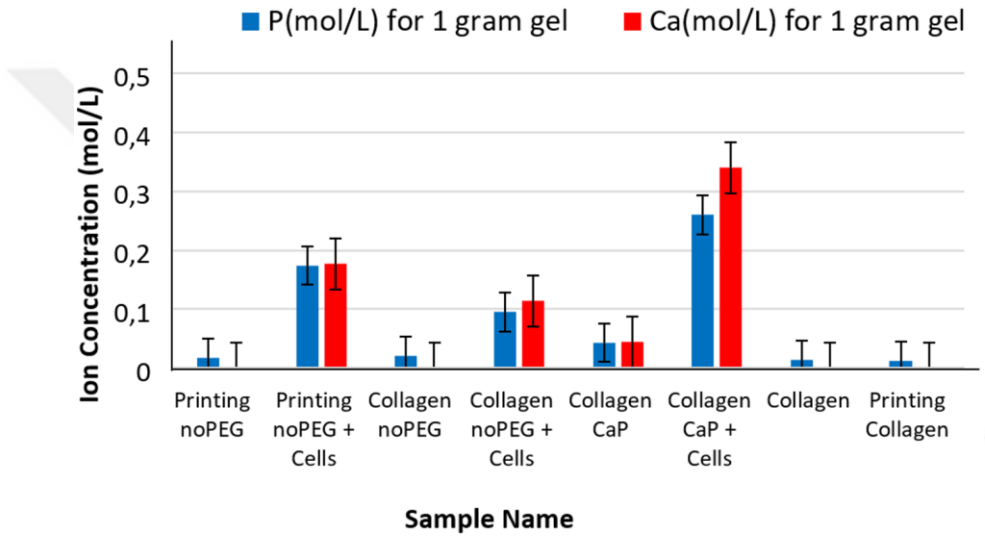


Figure 4.13 P and Ca ion concentration (mol/L) results of calcified EV-cell gels obtained by ICP-MS after 2 weeks of incubation

Since the EVs were damaged in this study, a comparison between EVs gels and EVs-cell gels in terms of CaP production cannot be made. To see the effect of adding osteoblast cells to the gels on CaP production, the ICP-MS results of the printing collagen-noPEG EVs gels and standard collagen-noPEG EVs gels obtained in the previous gel study were compared with the ICP-MS results of the printing collagen-noPEG EVs-cell gels and the standard collagen-noPEG EVs-cell gels obtained in this gel study. As shown in Figure 4.14, an increase in Ca and P ion concentration was observed when osteoblast cells were added to both standard collagen-noPEG EVs gels and printing collagen-noPEG EVs gels. Therefore, it can be concluded that the addition of osteoblasts to collagen gels has a positive effect on CaP production.

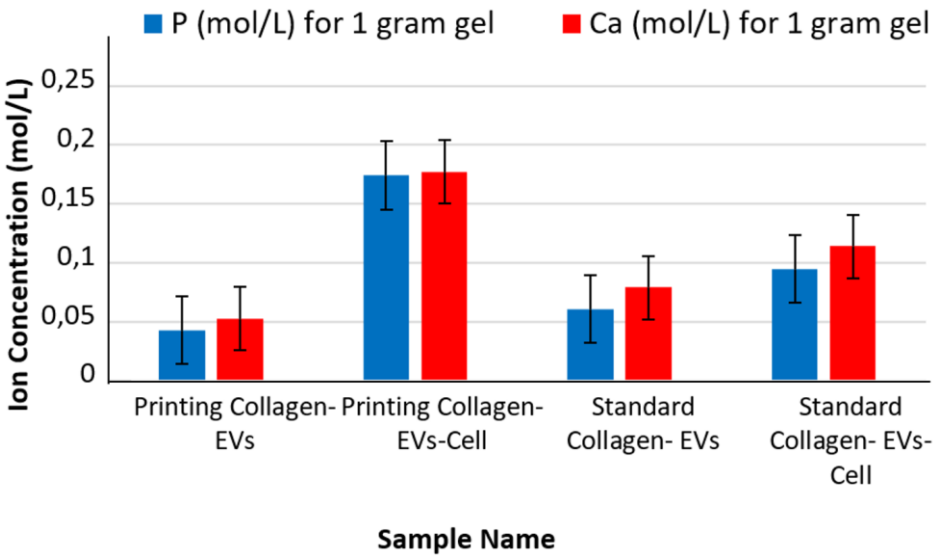


Figure 4.14 P and Ca ion concentration (mol/L) results of calcified EV gels with and without cells obtained by ICP-MS after 2 weeks of incubation

SEM was used to characterize the morphological structure of EV-cell gels and the particles formed. The SEM images are shown in Figure 4.15. While the thickness of the standard collagen fibers was measured to be approximately 150 ± 10 nm, the thickness of the printing collagen fibers was measured to be approximately 110 ± 8 nm.

Collagen structures and NPs structures attached to the gel surface were clearly observed in gels without cells. Since the sizes of the NPs observed in standard collagen-noPEG EVs (Figure 4.15.c), printing collagen-noPEG EVs (Figure 4.15.d), and standard collagen-CaP NPs gels (Figure 4.15.g) are between 400 and 900 nm. The SEM images of the majority of the studies in the literature also showed that the CaP NPs were in this size range [69, 70, 71]. Therefore, they are thought to be gel-generated CaP NP aggregates. The fact that EDX analysis performed on these particles (Figure 4.16, section c, d, e) also indicates the presence of Ca and P ions supports this claim.

Some irregularly shaped particle aggregates with bigger sizes compared to the literature studies (ranging from 3 to 7 μm) were found in printing collagen gel (Figure 4.15.b) and standard collagen-noPEG EVs gel (Figure 4.15.i). Since the EDX analyses (Figure 4.16.b) shows the presence of Ca and P ions, there is a possibility that they are CaP NPs aggregates. This possibility is supported by the fact that CaP NPs of similar size were obtained in the study by Guangqing and

colleagues [72].

It is known that CaP production in this study is related to the activity of osteoblast cells or EVs [16]. Therefore, it can be assumed that the cell-free gels mentioned above produce CaP primarily in the presence of EVs. However, as mentioned in the Discussion section where Figure 4.13 is explained, it is thought that the EVs in these gels may have been damaged and lost their CaP producing function. This strengthens the possibility that the CaP nanoparticles in these gels were formed by the random combination of ions taken from the differentiation medium during incubation. However, the presence of a few EVs that still retain their function may have triggered this. Apart from these possibilities and taking into account the margin of error in the EDX analysis, there remains the possibility that these NPs are dust resulting from contamination.

In addition, perfectly round particles, (Figure 15.a) with sizes ranging from 0.7 μm to 2 μm were observed in standard collagen gel. Although EDX analyses (Figure 16.a) confirmed the presence of Ca and P ions in the contents of these particles, the fact that they are too large to be perfectly round CaP NPs (not aggregates) [73] raises a question mark. Due to the similarity in size, shape, and ion content [74], it is considered possible that these are bacteria that came from the environment during incubation. As a result of the ICP-MS analysis at Figure 4.13, the absence of Ca and P ions in these gels strengthens the possibility of contamination.

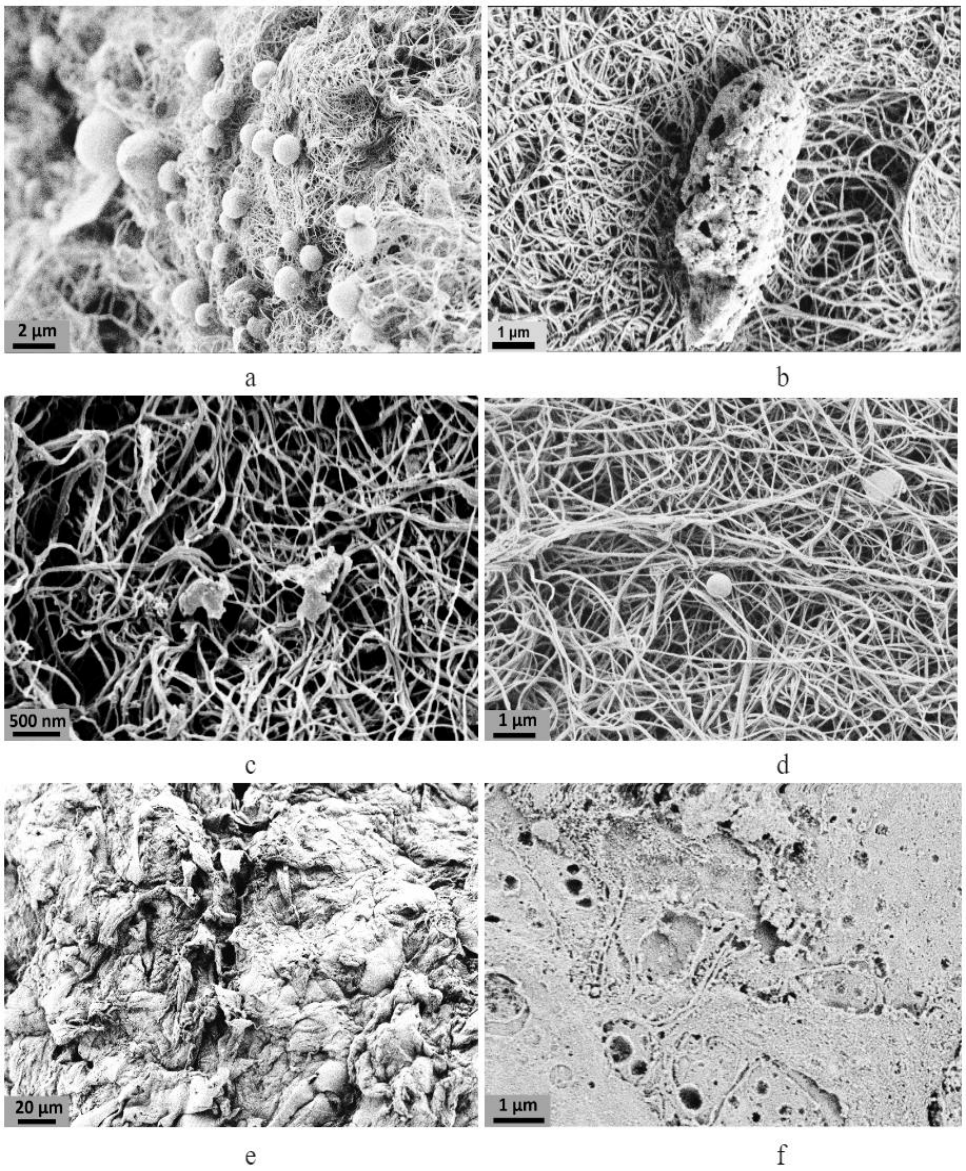


Figure 4.15 SEM images of the collagen-EV-cell gels, **a:** Standard collagen gel, **b:** Printing collagen gel, **c:** Standard collagen-noPEG EVs gel, **d:** Printing collagen-noPEG EVs gel, **e:** Standard collagen-noPEG EVs-cell gel, **f:** Printing collagen-noPEG EVs-cell gel

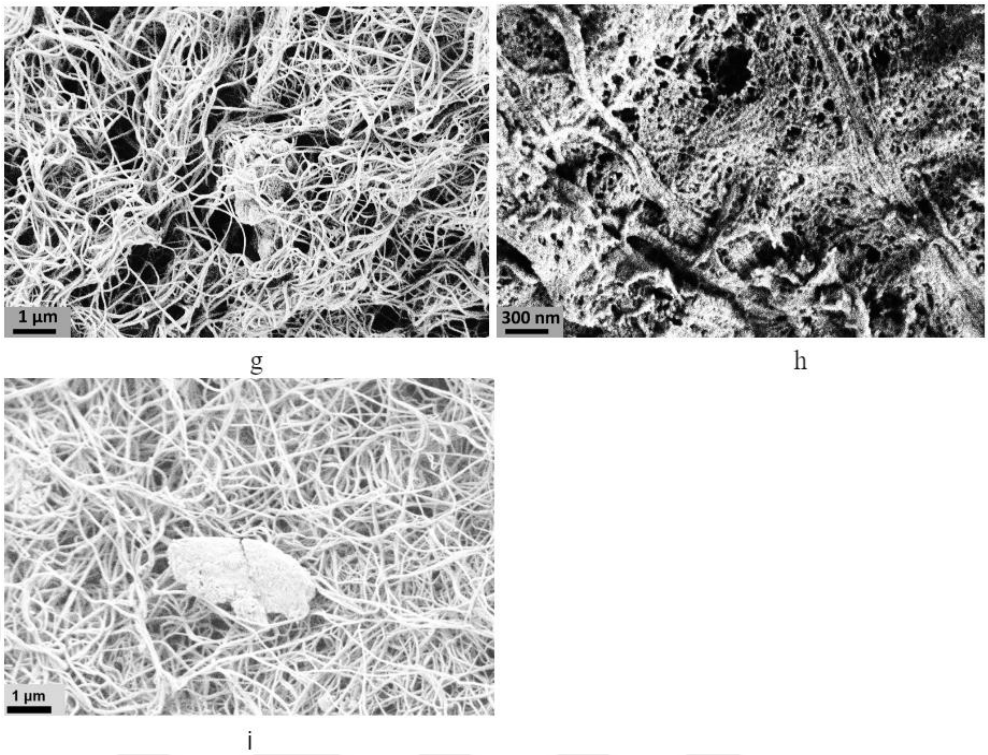


Figure 4.15 SEM images of the collagen-EV-cell gels (continued), **g:** Standard collagen-CaP NPs gel, **h:** Standard collagen-CaP NPs-cell gel, **i:** Standard collagen-noPEG EVs gel

On the other hand, in gels containing cells, fiber structures could not be observed because the cells surrounded the collagen structure and almost completely covered the outer surface. Based on the presence of porous structures in the SEM images (Figure 4.15 section f and h), and the dense morphological structure of the gels, it can be assumed that the osteoblast cells are completely integrated by contraction of the fibrous structure.

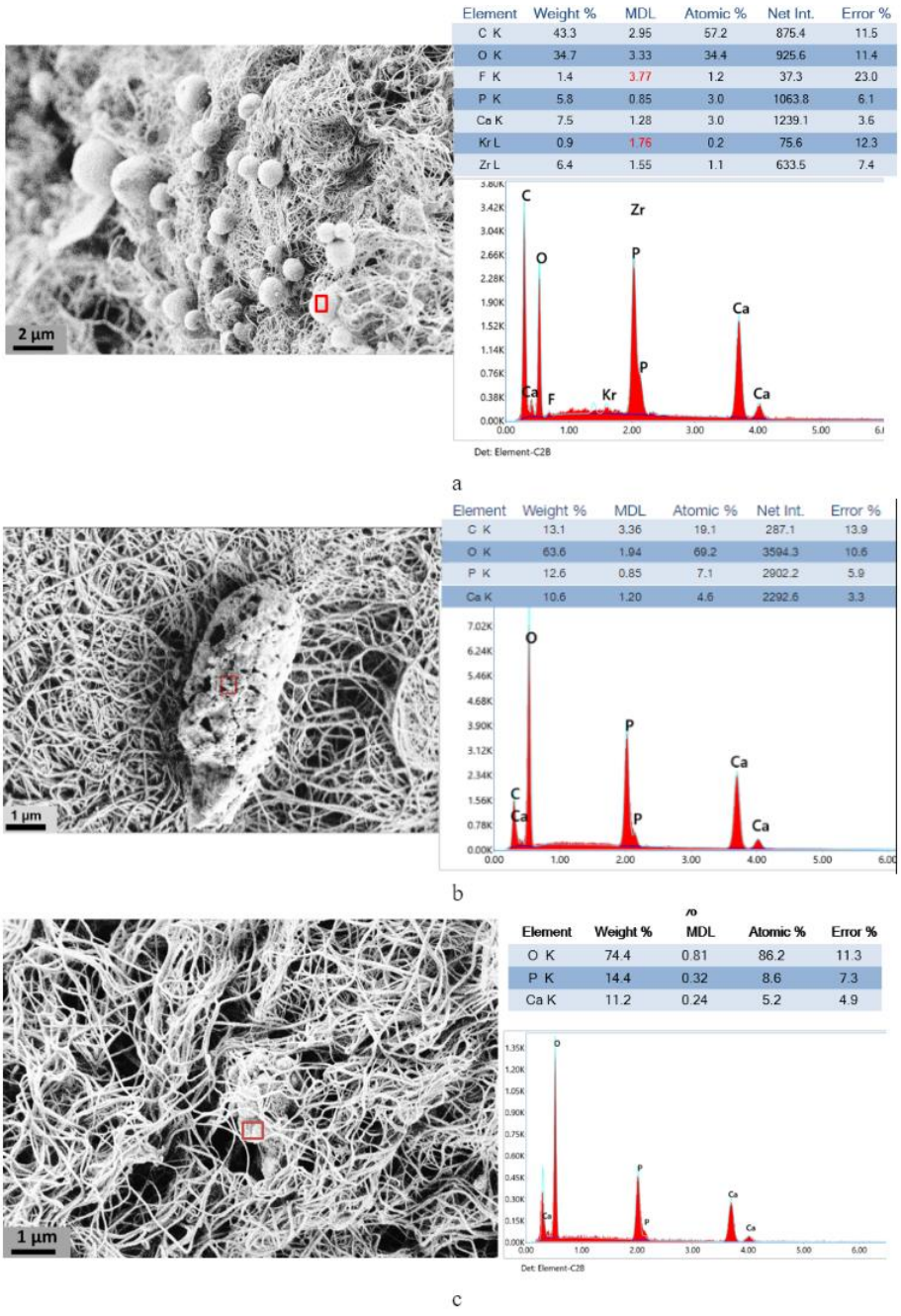


Figure 4.16 EDX analysis of the collagen-EV-cell gels, **a:** Standard collagen gel, **b:** Printing collagen gel, **c:** Standard collagen-CaP NPs gel

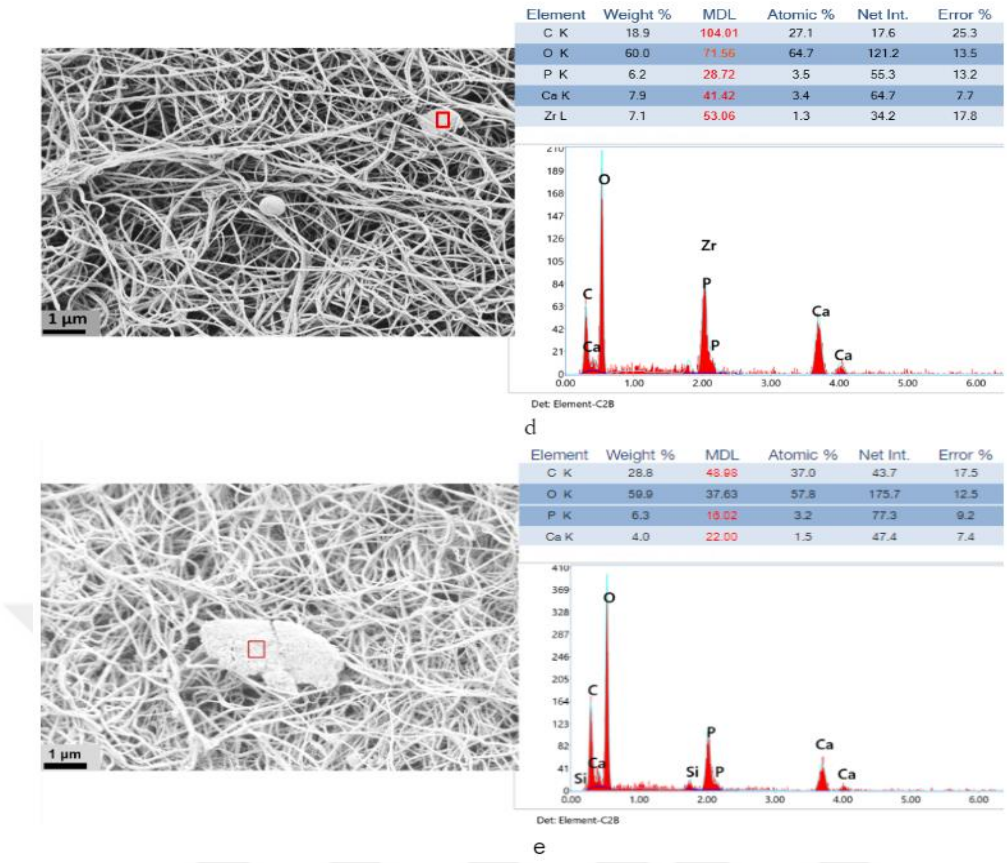


Figure 4.16 EDX analysis of the collagen-EV-cell gels (continued), **d:** Printing collagen-noPEG EVs gel, **e:** Standard collagen-noPEG EVs gel

Cross-sectional samples were taken from standard collagen-noPEG EVs-cell, standard collagen-CaP NPs-cell and printing collagen-noPEG EVs-cell gels and stained with alizarin red and DAPI. The results are shown in Figure 4.17. As no CaP NPs were found in gels without cells, both in ICP-MS and SEM results, the staining procedure was only applied to gels containing cells.

According to the results obtained, intense CaP accumulation was observed in the standard collagen-CaP NPs-cell gel sample. In addition, DAPI staining indicates a high concentration of cells. Considering that some of the observed CaP NPs were injected into the gel during the production phase, it can be concluded that the other NPs were produced by cells.

As mentioned above, since most of the EVs are likely to be damaged, it is assumed that the CaP NPs in the printing collagen-noPEG EVs-cell gel and the standard collagen-noPEG EVs- cell gel were produced by the osteoblast cells in these gels.

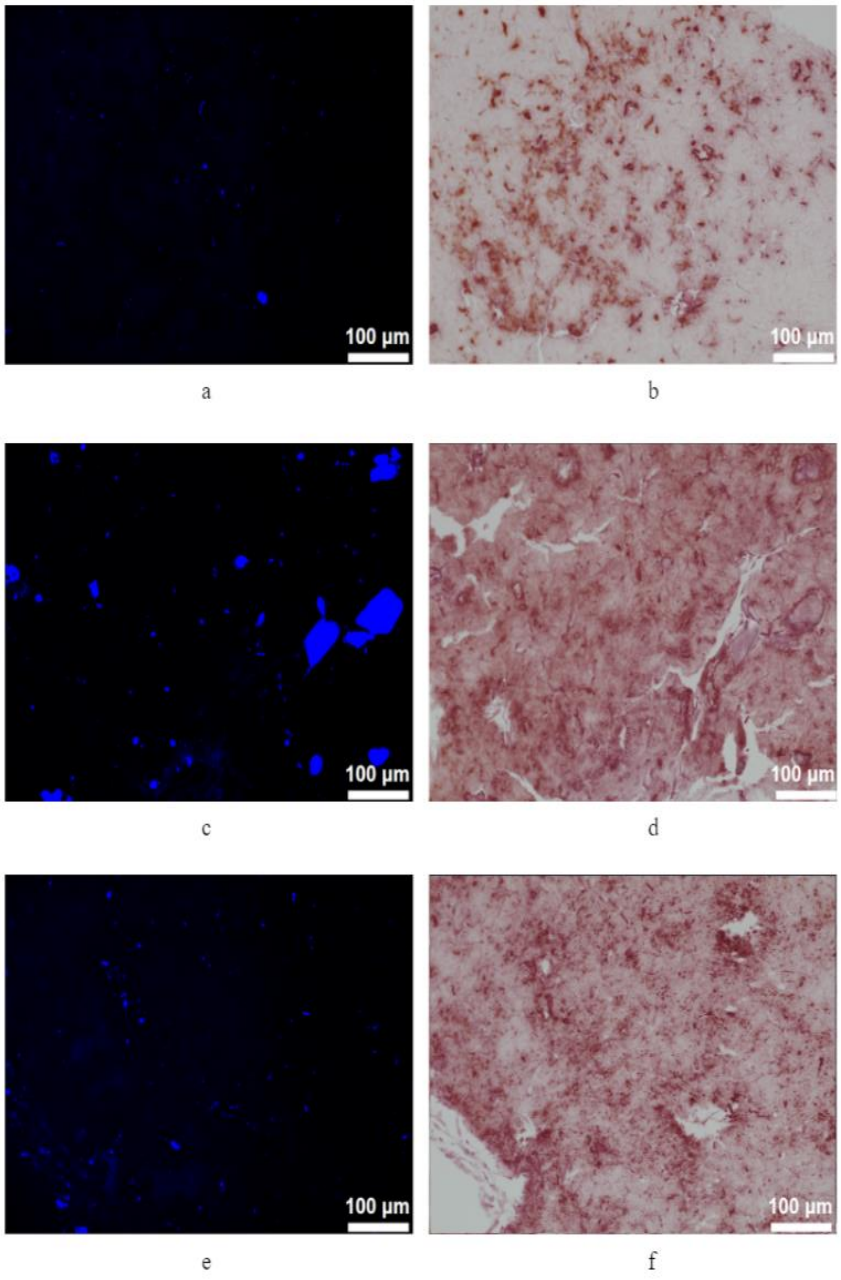


Figure 4.17 Light microscope images of collagen gels at 20X magnification after staining with alizarin red and DAPI, **a:** DAPI staining of standard collagen-noPEG EVs-cell, **b:** Alizarin red staining of standard collagen-noPEG EVs-cell, **c:** DAPI staining of standard collagen-CaP NPs-cell, **d:** Alizarin red staining of standard collagen-CaP NPs-cell, **e:** DAPI staining of printing collagen-noPEG EVs-cell, **f:** Alizarin red staining of printing collagen-noPEG EVs-cell

4.5 3-D Bioprinting Results

In order to test the biomimetic CaP production ability of the EVs and osteoblast cells, bone-like 3D bioprinting samples with EVs and osteoblast cells were manufactured. For this purpose, a collagen matrix was produced using isolated EVs, printing collagen and osteoblast cells. Bone-like 3D bioprinting samples were manufactured by using this collagen matrix.

3D bioprinted samples were incubated with differentiation medium for 4 weeks. Cross-sections were then taken from the 3D bioprinted samples and stained with alizarin red and DAPI to observe CaP NP production and cell presence. As shown in Figure 4.18, although the presence of some circular voids, a dense presence of CaP NPs was generally observed. It is thought that these circular spaces are the result of air bubbles formed during collagen matrix production. DAPI results indicated the presence of low density cells in all samples. The reason for this may be that the cells have been damaged during mixing with collagens or during the bioprinting process. The low cell presence means that only a small fraction of the observed CaP NPs is produced by cells, and it can be inferred that the remaining NPs are produced by EVs. Although the cell presence is below expectations, the fact that EVs effectively produce CaP NPs in the bone-like 3D bioprinted biomaterial allows us to conclude that they are successful in the biomimetic calcification process.

Comparing this result to the collagen EVs cell Alizarin Red and DAPI results shown in Figure 4.17, it is observed that the 3D bioprinted samples are lower in terms of both cell density and CaP NPs density. It is believed that the main reason for this difference is that the density of osteoblast cells and EVs is lower than in the collagen-EVs cell gels due to the presence of stabilization fibers and PCL grill layer used in the 3D bioprinted sample.

The manufactured 3D bioprinted samples showed that the isolated EVs produced CaP by successfully mimicking the physiological calcification process in a bone-like structure

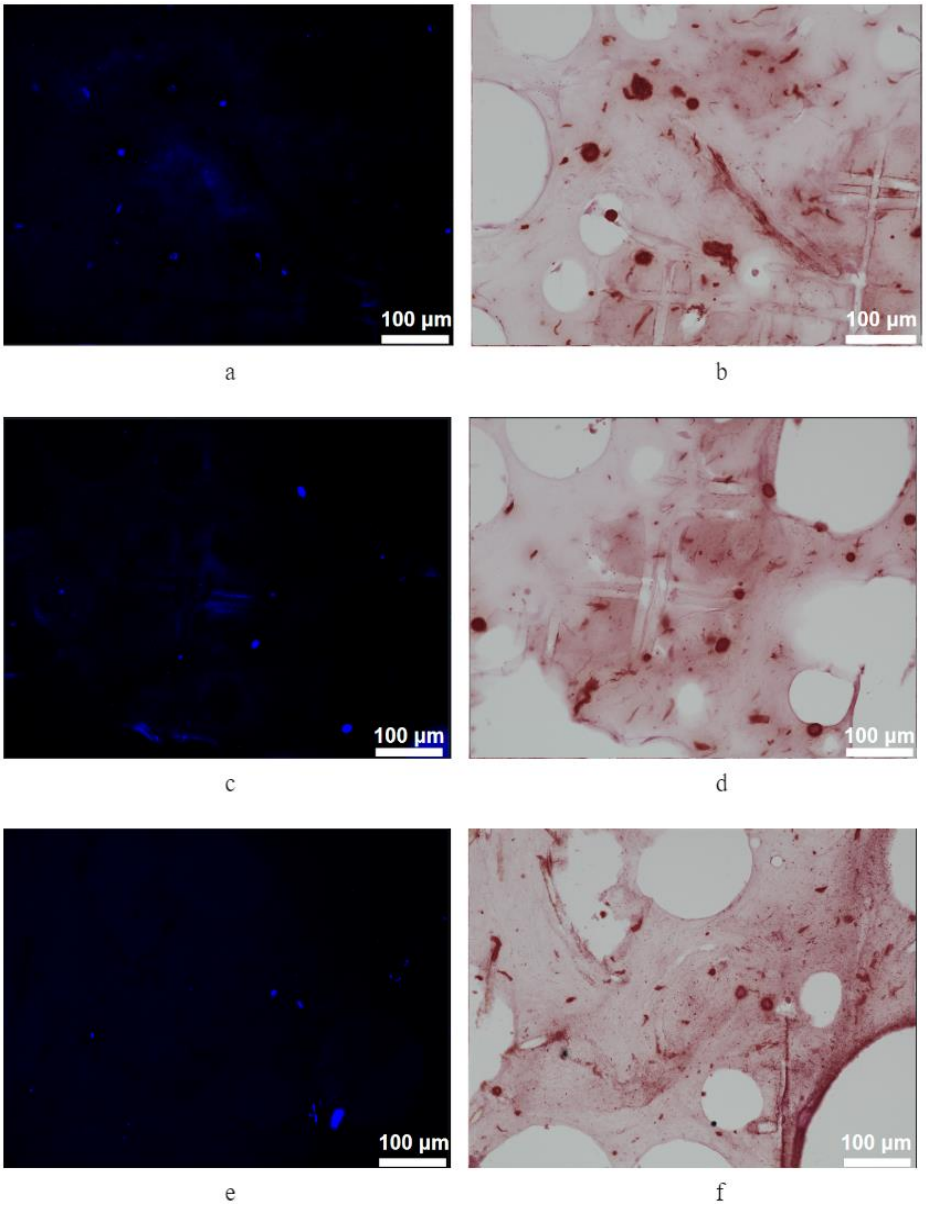


Figure 4.18 Light microscope images of bioprinted material samples at 20X magnification after staining with alizarin red and DAPI, **a:** DAPI staining of sample 1, **b:** Alizarin red staining of sample 1, **c:** DAPI staining of sample 2, **d:** Alizarin red staining of sample 2, **e:** DAPI staining of sample 3, **f:** Alizarin red staining of sample 3

5
CONCLUSION

In this study, EVs were isolated from osteoblast cells and their biomimetic CaP production was investigated in vitro. The following conclusions can be reached as a result of the experiments carried out in this study:

As a pre-experiment, CaP NPs were produced from osteoblast cells using 2D and 3D seeding environments. The characterization results from NTA and TEM showed that CaP NPs were generally spherical in shape and their size varies between 49 nm and 490 nm both for 2D and 3D seeding environments. The concentration of samples from 2D and 3D environments were $3.49 \times 10^9 \pm 8.2 \times 10^8$ particles/ml and $2.72 \times 10^9 \pm 2.6 \times 10^8$ particles/ml, respectively. It was determined that the seeding environment does not seem to have a significant effect on CaP NPs obtaining. Therefore, it was concluded that the 2D environment is more advantageous than the 3D environment because it is easier to use.

EVs were isolated from osteoblast cells using standard ultracentrifugation and PEG-precipitated ultracentrifugation methods. According to the ICP-MS results, no Ca and P ions were found in the EVs samples, which is an indication that the EVs were isolated before converted to CaP. NTA characterization showed that average mean size of EVs obtained with PEG precipitation method and non-PEG precipitation method were 215 ± 35 nm and 240 ± 32 nm, respectively. The average concentration values were $2.3 \times 10^{10} \pm 1.2 \times 10^{10}$ particles/mL) for PEG precipitation method and $1.2 \times 10^{10} \pm 1.1 \times 10^{10}$ particles/mL for non-PEG precipitation method. The results showed that approximately 91% more EVs were obtained with PEG precipitation method.

Isolated EVs were combined with 2 different synthetic collagen fibers to form gels. After 2 weeks of incubation, in both the alizarin red staining and ICP-MS results, it was observed that gels formed with no-PEG EVs produced more CaP than gels formed with PEG EVs. Therefore, the non-PEG precipitation method was concluded to be more advantageous, even though fewer EVs can be obtained with this method.

A collagen matrix was produced using isolated EVs, synthetic collagen fibers and human osteoblast cells. This collagen matrix was used to manufacture bone-like 3D

bioprinted samples. Using alizarin red staining after 4 weeks of incubation, it was observed that isolated EVs produced CaP NPs by successfully mimicking the physiological calcification process in bone-like structures. The DAPI staining study displayed that the osteoblast cells were adhered on bioprinting fibers and contributed to CaP production by releasing EVs.

Considering the findings in this study, it was shown that the isolated EVs from osteoblasts have ability to produce biomimetic CaP NPs when they are cooperated with collagen fibers and 3D bioprinted samples. We believe that our study will breathe new life into the literature on biomimetic CaP fabrication. In this way, the biocompatibility problems encountered in bone grafting can be overcome and the quality of life of many people who have difficulties in this regard can be improved

Further studies are planned to develop the integration of osteoblast cells and EVs into the 3D bioprinted samples. For this, the bioprinting process is considered to be repeated by changing the parameters such as pressure, stabilizer fiber properties used, and collagen matrix formation. Furthermore, future studies will incorporate SEM characterization to better understand the morphological structure of 3D bioprinted samples. In addition, to increase the efficiency of EVs isolation, it is planned to repeat the current isolation methods with different parameters or to use new methods to compare the efficiency.

REFERENCES

[1] Singh, Gurdyal et al. “Customized hydroxyapatites for bone-tissue engineering and drug delivery applications: a review.” Journal of Sol-Gel Science and Technology 94 (2020): 505-530.

[2] Sanan A, Haines SJ. Repairing Holes in the Head. “A History of Cranioplasty. Neurosurgery.” 1997 Mar;40(3):588.

[3] Feroz S, Cathro P, ivanovski S, Muhammad N. “Biomimetic bone grafts and substitutes: A review of recent advancements and applications” Biomedical Engineering Advances. 2023 Nov 1;6:100107.

[4] Vieira VSJG da Rosa ÂR, Montagner PG, de Campos FUF, Teixeira LN, Aura JM, et al. “Effect of ozone therapy on the modulation of inflammation and on new bone formation in critical defects of rat calvaria filled with autogenous graft.” Journal of Stomatology, Oral and Maxillofacial Surgery. 2023 Feb 1;124 (1, Supplement): 192

[5] Norman-Taylor FH, Santori N, Villar RN. “The trouble with bone allograft: We need a safe, abundant alternative.” BMJ. 1997 Aug 30;315(7107):498.

[6] Bracey DN, Seyler TM, Jinnah AH, Smith TL, Ornelles DA, Deora R, et al. “A porcine xenograft-derived bone scaffold is a biocompatible bone graft substitute: An assessment of cytocompatibility and the alpha-Gal epitope. Xenotransplantation.” 2019;26(5):e12534.

[7] Greenwald AS, Boden SD, Goldberg VM, Khan Y, LaurencinCT, et al. “Bone-Graft Substitutes: Facts, Fictions, and Applications.” JBJS. 2001 Nov;83(2): S98.

[8] Demers C, Hamdy CR, Corsi K, Chellat F, Tabrizian M, Yahia L. “Natural coral exoskeleton as a bone graft substitute: a review” Biomed Mater Eng. 2002;12(1):15-35. PMID: 11847406.

[9] Vangsness CT, Wagner PP, Moore TM, Roberts MR. “Overview of Safety issues Concerning the Preparation and Processing of Soft-Tissu Allografts. Arthroscopy” The Journal of Arthroscopic & Related Surgery. 2006 Dec 1;22(12):1351–8.

[10] Nauth, A.; Schemitsch, E.; Norris, B.; Nollin, Z.; Watson, J.T. “Critical- Size Bone Defects: Is There a Consensus for Diagnosis and Treatment?” J. Orthop. Trauma 2018, 32 (Suppl. 1), S7–S11.

[11] Monroe, E.; Bass, D.; Votava, W.; Mc Mullen, J. “New calcium phosphate ceramic material for bone and tooth implants.” J. Dent Res. 1971, 50, 860–861.

[12] Hou X, Zhang L, Zhou Z, Luo X, Wang T, Zhao X, Lu B, Chen F, Zheng L. “Calcium Phosphate-Based Biomaterials for Bone Repair.” J Funct Biomater. 2022 Oct 14;13(4):187. doi: 10.3390/jfb13040187. PMID: 36278657; PMCID: PMC9589993.

[13] Singh, Gurdyal et al. “Customized hydroxyapatites for bone-tissue engineering and drug delivery applications: a review.” Journal of Sol-Gel Science and Technology 94 (2020): 505-530.

[14] Zhou H, Lee J. “Nanoscale hydroxyapatite particles for bone tissue engineering.” Acta Biomater. 2011 Jul;7(7):2769-81. doi: 10.1016/j.actbio.2011.03.019. Epub 2011 Apr 1. PMID: 21440094.

[15] Zhao R, Yang R, Cooper PR, Khurshid Z, Shavandi A, Ratnayake J. “Bone Grafts and Substitutes in Dentistry: A Review of Current Trends and Developments. Molecules.” 2021; 26(10):3007. https://doi.org/10.3390/molecules26103007

[16] Ansari S, de Wildt BWM, Vis MAM, de Korte CE, Ito K, Hofmann S, Yuana Y. “Matrix Vesicles: Role in Bone Mineralization and Potential Use as Therapeutics.” Pharmaceuticals (Basel). 2021 Mar 24;14(4):289. doi: 10.3390/ph14040289. PMID: 33805145; PMCID: PMC8064082.

[17] Abels ER, Breakefield XO. “Introduction to Extracellular Vesicles: Biogenesis, RNA Cargo Selection, Content, Release, and Uptake.” Cell Mol Neurobiol. 2016 Apr;36(3):301-12. doi: 10.1007/s10571-016-0366-z. Epub 2016 Apr 6. PMID: 27053351; PMCID: PMC5546313.

[18] Zhang P, Yeo JC, Lim CT. “Advances in Technologies for Purification and Enrichment of Extracellular Vesicles”. SLAS Technol. 2019 Oct;24(5):477-488. doi: 10.1177/2472630319846877. Epub 2019 May 14. PMID: 31088199.

[19] Börger V, Staubach S, Dittrich R, Stambouli O, Giebel B. “Scaled Isolation of Mesenchymal Stem/Stromal Cell-Derived Extracellular Vesicles.” Curr Protoc Stem Cell Biol. 2020 Dec;55(1):e128. doi: 10.1002/cpsc.128. PMID: 32956560.

[20] Al-Sharabi N, Mohamed-Ahmed S, Shanbhag S, Kampleitner C, Elnour R, Yamada S, Rana N, Birkeland E, Tangl S, Gruber R, Mustafa K. “Osteogenic human MSC-derived extracellular vesicles regulate MSC activity and osteogenic differentiation and promote bone regeneration in a rat calvarial defect model.” Stem Cell Res Ther. 2024 Feb 7;15(1):33. doi: 10.1186/s13287-024-03639-x. PMID: 38321490; PMCID: PMC10848378.

[21] Clarke B. (2008). “Normal bone anatomy and physiology. Clinical journal of the American Society of Nephrology” CJASN, 3 Suppl 3(Suppl 3), S131–S139. https://doi.org/10.2215/CJN.04151206

[22] Albee FH. “Studies in bone growth” Ann Surg. 1920 Jan; 71 (1): 32–9.

[23] Al-Sanabani JS, Madfa AA, Al-Sanabani FA.“Application of Calcium Phosphate Materials in Dentistry.” International Journal of Biomaterials. 2013 Jun 26;2013: e87

[24] Epple M, Ganesan K, Heumann R, Klesing J, Kovtun A, Neumann S, et al. “Application of calcium phosphate nanoparticles in biomedicine.” Journal of Materials Chemistry. 2010;20(1):18–23.

[25] Szcześ A, Hołysz L, Chibowski E. “Synthesis of hydroxyapatite for biomedical applications” Advances in Colloid and interface Science. 2017 Nov 1;249:321–30.

[26] LeGeros RZ, Lin S, Rohanizadeh R, Mijares D, LeGeros JP. “Biphasic calcium phosphat bioceramics: preparation, properties and applications.” Journal of Materials Science: Materials in Medicine. 2003 Mar 1;14(3):201–9.

[27] Gao L, Liu G, Wu X, Liu C, Wang Y, Ma M, et al. “Osteocytes autophagy mediated by mTORC2 activation controls osteoblasts differentiation and osteoclasts activities under mechanical loading” Archives of Biochemistry and Biophysics. 2023 Jul1;742 :109634.

[28] Kim, J. M., Lin, C., Stavre, Z., Greenblatt, M. B., & Shim, J. H. (2020). “Osteoblast-Osteoclast Communication and Bone Homeostasis.” Cells, 9(9), 2073. https://doi.org/10.3390/cells9092073

[29] Siddiqui JA, Partridge NC. “Physiological Bone Remodeling: Systemic Regulation and Growth Factor involvement.” Physiology. 2016 May;31(3):233–45.

[30] Feroz S, Cathro P, ivanovski S, Muhammad N. “Biomimetic bone grafts and substitutes: A review of recent advancements and applications.” BiomedicalEngineering Advances. 2023 Nov 1;6:100107.

[31] Battafarano G, Rossi M, De Martino V, Marampon F, Borro L, Secinaro A, Del Fattore A. “Strategies for Bone Regeneration: From Graft to Tissue Engineering.” International Journal of Molecular Sciences. 2021; 22(3):1128. https://doi.org/10.3390/ijms2203112

[32] Orlovskii VP, Komlev VS, Barinov SM. “Hydroxyapatite and Hydroxyapatite- Based Ceramics.” Inorganic Materials. 2002 Oct 1;38(10):973–84.

[33] Schilling AF, Linhart W, Filke S, Gebauer M, Schinke T, Rueger JM, Amling M. “Resorbability of bone substitute biomaterials by human osteoclasts.” Biomaterials. 2004 Aug;25(18):3963-72. doi: 10.1016/j.biomaterials.2003.10.079. PMID: 15046886.

[34] Witwer KW, Théry C. “Extracellular vesicles or exosomes? On primacy, precision, and popularity influencing a choice of nomenclature.” J Extracell Vesicles. 2019 Aug 1;8(1):1648167. doi: 10.1080/20013078.2019.1648167. PMID: 31489144; PMCID: PMC6711079.

[35] DISPERTECH, “What are extracellular vesicles?”, retrieved 2023, from https://dispertech.com/applications/extracellular-vesicles-evs/

[36] Kooijmans SAA, Fliervoet LAL, van der Meel R, Fens MHAM, Heijnen HFG, van Bergen En Henegouwen PMP, Vader P, Schiffelers RM. “PEGylated and targeted extracellular vesicles display enhanced cell specificity and circulation time.” J Control Release. 2016 Feb 28;224:77-85. doi: 10.1016/j.jconrel.2016.01.009. Epub 2016 Jan 7. PMID: 26773767.

[37] E. Ersöz, O. B. Can, ve S. Uzunoğlu, “Eksozomların Kanserdeki Rolü”, CBU-SBED, c. 3, sy. 1, ss. 144–152, 2016.

[38] Keshtkar S, Azarpira N, Ghahremani MH. “Mesenchymal stem cell-derived extracellular vesicles: novel frontiers in regenerative medicine.” Stem Cell Res Ther. 2018 Mar 9;9(1):63. doi: 10.1186/s13287-018-0791-7. PMID: 29523213; PMCID: PMC5845209.

[39] Yu L, Zhu G, Zhang Z, Yu Y, Zeng L, Xu Z, Weng J, Xia J, Li J, Pathak JL. “Apoptotic bodies: bioactive treasure left behind by the dying cells with robust diagnostic and therapeutic application potentials.” J Nanobiotechnology. 2023

Jul 12;21(1):218. doi: 10.1186/s12951-023-01969-1. PMID: 37434199; PMCID: PMC10337089.

[40] Clarke B. “Normal bone anatomy and physiology.” Clin J Am Soc Nephrol. 2008 Nov;3 Suppl 3(Suppl 3):S131-9. doi: 10.2215/CJN.04151206. PMID: 18988698; PMCID: PMC3152283.

[41] BECKMAN COULTER, “Optima MAX-XP, Ultracentrifuge”, retrieved 2016 February 20, from https://goto.beckman.com/en/ultracentrifugation-density-gradient-centrifugation/?campaign

[42] Momen-Heravi F, Balaj L, Alian S, Mantel PY, Halleck AE, Trachtenberg AJ, Soria CE, Oquin S, Bonebreak CM, Saracoglu E, Skog J, Kuo WP. “Current methods for the isolation of extracellular vesicles.” Biol Chem. 2013 Oct;394(10):1253-62. doi: 10.1515/hsz-2013-0141. PMID: 23770532; PMCID: PMC7075462.

[43] Weng Y, Sui Z, Shan Y, Hu Y, Chen Y, Zhang L, Zhang Y. “Effective isolation of exosomes with polyethylene glycol from cell culture supernatant for in-depth proteome profiling.” Analyst. 2016 Aug 7;141(15):4640-6. doi: 10.1039/c6an00892e. Epub 2016 May 27. PMID: 27229443.

[44] Dantas-Lima JJ, Corteel M, Cornelissen M, Bossier P, Sorgeloos P, Nauwynck HJ. “Purification of white spot syndrome virus by iodixanol density gradient centrifugation.” J Fish Dis. 2013 Oct;36(10):841-51. doi: 10.1111/jfd.12082. Epub 2013 Feb 6. PMID: 23384051.

[45] Yang D, Zhang W, Zhang H, Zhang F, Chen L, Ma L, Larcher LM, Chen S, Liu N, Zhao Q, Tran PHL, Chen C, Veedu RN, Wang T. “Progress, opportunity, and perspective on exosome isolation- efforts for efficient exosome-based theranostics.” Theranostics. 2020 Feb 19;10(8):3684-3707. doi: 10.7150/thno.41580. PMID: 32206116; PMCID: PMC7069071.

[46] Barth, Howard & Boyes, Barry & Jackson, Christian. (2010). “Size Exclusion Chromatography and Related Separation Techniques.” Cheminform. 29. 10.1002/chin.199834345.

[47] Sagar Aryal, “Gel Filtration Chromatography- Definition, Principle, Types, Parts, Steps, Uses”, retrieved 2022 January 26, from https://microbenotes.com/gel-filtration-chromatography/

[48] Della Bona A, Cantelli V, Britto VT, Collares KF, Stansbury JW. “3D printing restorative materials using a stereolithographic technique: a systematic review.” Dent Mater. 2021 Feb;37(2):336-350. doi: 10.1016/j.dental.2020.11.030. Epub 2021 Jan 19. PMID: 33353734; PMCID: PMC7855936.

[49] Aimar A, Palermo A, Innocenti B. “The Role of 3D Printing in Medical Applications: A State of the Art.” J Healthc Eng. 2019 Mar 21;2019:5340616. doi: 10.1155/2019/5340616. PMID: 31019667; PMCID: PMC6451800.

[50] Bajaj P, Schweller RM, Khademhosseini A, West JL and Bashir R, Annu. Rev. Biomed. Eng, 2014, 16, 247–276. [PMC free article] [PubMed] [Google Scholar]

[51] Groll J, Boland T, Blunk T, Burdick JA, Cho D-W, Dalton PD, Derby B, Forgacs G, Li Q, Mironov VA, Moroni L, Nakamura M, Shu W, Takeuchi S,

Vozzi G, Woodfield TBF, Xu T, Yoo JJ and Malda J, Biofabrication, 2016, 8, 013001. [PubMed] [Google Scholar]

[52] Murphy SV and Atala A, Nat. Biotechnol, 2014, 32, 773–785. [PubMed] [Google Scholar]

[53] Carrow JK, Kerativitayanan P, Jaiswal MK, Lokhande G and Gaharwar AK, "in Essentials of 3D Biofabrication and Translation," ed. Yoo AAJ, Academic Press, Boston, 2015, pp. 229–248. [Google Scholar]

[54] Gungor-Ozkerim PS, Inci I, Zhang YS, Khademhosseini A, Dokmeci MR . "Bioinks for 3D bioprinting: an overview." Biomater Sci. 2018 May 1;6(5):915-946. doi: 10.1039/c7bm00765e. PMID: 29492503; PMCID: PMC6439477.

[55] Lee HJ, Kim YB, Ahn SH, Lee J-S, Jang CH, Yoon H, Chun W and Kim GH, Adv. Healthcare Mater, 2015, 4, 1359–1368. [PubMed] [Google Scholar]

[56] Loo Y, Lakshmanan A, Ni M, Toh LL, Wang S and Hauser CAE, Nano Lett, 2015, 15, 6919–6925. [PubMed] [Google Scholar]

[57] Sigaux N, Pourchet L, Breton P, Brosset S, Louvrier A, Marquette CA. "3D Bioprinting: principles, fantasies and prospects." J Stomatol Oral Maxillofac Surg. 2019 Apr;120(2):128-132. doi: 10.1016/j.jormas.2018.12.014. Epub 2019 Jan 1. PMID: 30609384.

[58] Weigel T, Malkmus C, Weigel V, Wußmann M, Berger C, Brennecke J, Groeber-Becker F, Hansmann J. "Fully Synthetic 3D Fibrous Scaffolds for Stromal Tissues-Replacement of Animal-Derived Scaffold Materials Demonstrated by Multilayered Skin." Adv Mater. 2022 Mar;34(10):e2106780. doi: 10.1002/adma.202106780. Epub 2022 Jan 21. PMID: 34933407.

[59] Ludwig AK, De Miroschedji K, Doeppner TR, Börger V, Ruesing J, Rebmann V, Durst S, Jansen S, Bremer M, Behrmann E, Singer BB, Jastrow H, Kuhlmann JD, El Magraoui F, Meyer HE, Hermann DM, Opalka B, Raunser S, Epple M, Horn PA, Giebel B. "Precipitation with polyethylene glycol followed by washing and pelleting by ultracentrifugation enriches extracellular vesicles from tissue culture supernatants in small and large scales." J Extracell Vesicles. 2018 Oct 17;7(1):1528109. doi: 10.1080/20013078.2018.1528109. PMID: 30357008; PMCID: PMC6197019.

[60] Xie J, Riley C, Chittur K. "Effect of albumin on brushite transformation to hydroxyapatite." J Biomed Mater Res. 2001 Dec 5;57(3):357-65. doi:10.1002/1097-4636(20011205)57:3<357::aid-jbm1178>3.0.co;2-1. PMID: 11523030.

[61] Ataol, S., Tezcaner, A., Duygulu, O. et al. "Synthesis and characterization of nanosized calcium phosphates by flame spray pyrolysis, and their effect on osteogenic differentiation of stem cells." J Nanopart Res 17, 95 (2015). https://doi.org/10.1007/s11051-015-2901-

[62] Margolis HC, Kwak SY, Yamazaki H. "Role of mineralization inhibitors in the regulation of hard tissue biomineralization: relevance to initial enamel formation and maturation." Front Physiol. 2014 Sep 10;5:339. doi: 10.3389/fphys.2014.00339. PMID: 25309443; PMCID: PMC4159985.

[63] Liu, X., & K., S. (2011). “Bioinspired Synthesis of Organic/Inorganic Nanocomposite Materials Mediated by Biomolecules.” InTech. doi: 10.5772/18411

[64] Kwak SY, Wiedemann-Bidlack FB, Beniash E, Yamakoshi Y, Simmer JP, Litman A, Margolis HC. Role of 20-kDa amelogenin (P148) “Phosphorylation in calcium phosphate formation in vitro.” J Biol Chem. 2009 Jul 10;284(28):18972-9. doi: 10.1074/jbc.M109.020370. Epub 2009 May 14. PMID: 19443653; PMCID: PMC2707234.

[65] Zhen K, Wei X, Zhi Z, Zhang S, Cui L, Li Y, Chen X, Yao J, Zhang H. “Comparison of Different Isolation Methods for Plasma-Derived Extracellular Vesicles in Patients with Hyperlipidemia.” Life (Basel). 2022 Nov 21;12(11):1942. doi: 10.3390/life12111942. PMID: 36431076; PMCID: PMC9692895.

[66] Otani K, Fujioka Y, Okada M, Yamawaki H. “Optimal Isolation Method of Small Extracellular Vesicles from Rat Plasma.” Int J Mol Sci. 2019 Sep 26;20(19):4780. doi: 10.3390/ijms20194780. PMID: 31561474; PMCID: PMC6801590.

[67] Gámez-Valero A, Monguió-Tortajada M, Carreras-Planella L, Franquesa Ml, Beyer K, Borràs FE. “Size-Exclusion Chromatography-based isolation minimally alters Extracellular Vesicles' characteristics compared to precipitating agents.” Sci Rep. 2016 Sep 19;6:33641. doi: 10.1038/srep33641. PMID: 27640641; PMCID: PMC5027519.

[68] Zhao, M., Su, R., Ji, L., Zhang, Y., Wu, H., Wen, Z., & Dai, C. (2023). “The Biocompatibility and Antibacterial Properties of the CNTs-Doped Magnesium Based Composite Implants in a Long-Term Biodegradation Process.” Journal of Nanomaterials.

[69] Ganesan, Kathirvel & Vikman, Anna & Neumann, Sebastian & Heumann, Rolf & Epple, Matthias. (2008). “Calcium phosphate nanoparticles: Colloidally stabilized and made fluorescing by a phosphate-functionalized porphyrin.” Journal of Materials Chemistry. 18. 3655-3661. 10.1039/B805366A.

[70] Tas AC . “X-ray-amorphous calcium phosphate (ACP) synthesis in a simple biomineralization medium”. J Mater Chem B. 2013 Sep 21;1(35):4511-4520. doi: 10.1039/c3tb20854k. Epub 2013 Jul 29. PMID: 32261124.

[71] Wagner DE, Eisenmann KM, Nestor-Kalinoski AL, Bhaduri SB. “A microwave-assisted solution combustion synthesis to produce europium-doped calcium phosphate nanowhiskers for bioimaging applications.” Acta Biomater. 2013 Sep;9(9):8422-32. doi: 10.1016/j.actbio.2013.05.033. Epub 2013 Jun 11. PMID: 23764803.

[72] Liu, Guangqing & Xue, Mengwei & Liu, Qinpu & Zhou, Yuming. (2017). “Acrylic acid–allylpolyethoxy carboxylate copolymer as a environmentally friendly scale inhibitor (part II).” Clean Technologies and Environmental Policy. 19. 10.1007/s10098-016-1258-0

[73] Khalifehzadeh R, Arami H. “Biodegradable calcium phosphate nanoparticles for cancer therapy.” Adv Colloid Interface Sci. 2020 May; 279:102157. doi:

10.1016/j.cis.2020.102157. Epub 2020 Apr 10. PMID: 32330734; PMCID: PMC7261203.

[74] Taylor JA, Sichel SR, Salama NR. “Bent Bacteria: A Comparison of Cell Shape Mechanisms in Proteobacteria.” Annu Rev Microbiol. 2019 Sep 8;73:457-480. doi: 10.1146/annurev-micro-020518-115919. Epub 2019 Jun 14. PMID: 31206344.

PUBLICATIONS FROM THE THESIS

Orak M., Hoeppel A., Weigel T, Dembski S., Özmen M.M, “Biomimetic Synthesis and Characterization of Calcium Phosphate Nanoparticles for Regenerative Medicine", The 4th International Congress of Engineering and Natural Sciences, Ankara, Turkey, May 24-25, 2024.